

Synthetic Face Datasets Generation via Latent Space Exploration from Brownian Identity Diffusion

David Geissbühler, Hatef Otrosi Shahreza, and Sébastien Marcel

Abstract—Face Recognition (FR) models are trained on large-scale datasets, which have privacy and ethical concerns. Lately, the use of synthetic data to complement or replace genuine data for the training of FR models has been proposed. While promising results have been obtained, it still remains unclear if generative models can yield diverse enough data for such tasks. In this work, we introduce a new method, inspired by the physical motion of soft particles subjected to stochastic Brownian forces, allowing us to sample identities distributions in a latent space under various constraints. With this in hands, we generate several face datasets and benchmark them by training FR models, showing that data generated with our method exceeds the performance of previously GAN-based datasets and achieves competitive performance with state-of-the-art diffusion-based synthetic datasets. We also show that this method can be used to mitigate leakage from the generator’s training set and explore the ability of generative models to generate data beyond it.

Index Terms—Brownian Identity Diffusion, Face Recognition, Latent Space, Synthetic Dataset.



1 INTRODUCTION

Deep learning (DL) [1] is perhaps one of the most impactful scientific achievement of the last decades. Machine learning (ML), often dubbed artificial intelligence (AI) in the popular literature, aims at uncovering hidden patterns and complex correlations in large volumes of data whose features span high dimensional spaces. According to the DL paradigm, given a *deep enough* architecture and given sufficient training data, almost arbitrarily high accuracy can be achieved by such models. The recent advent of inexpensive compute hardware has made both training and inference of very large ML models, with several billions of hyper-parameters, tractable, even on consumer grade devices. This has led to an exponential pace for the deployment of such algorithms, in applications ranging from computer vision (CV) to natural language processing (NLP). However, while the design of such systems is now well understood, it is becoming increasingly challenging to develop better models as more and more training data is required.

Real-world data, in particular biometric ones, can possibly contain sensitive information which raises privacy concerns from both legal and ethical specialists [2]. This is particularly true for a number of large biometric datasets that have been collected *in the wild*, for instance by scraping images from the internet. Moreover, in addition to privacy concerns, biometric data might give a biased representation of the population depending on the data collection procedure [3]. Recently, MS-Celeb [4], a very popular dataset

commonly used to train FR models, was withdrawn after exposure in the media of its privacy, fairness and demographic biases problems. While data collection campaigns performed in laboratories can be made representative of the general demographics and performed with subjects consents, they are typically quite limited due to the large amount of effort they require.

In this work, we propose another step towards the tackling of some of these issues by developing physics-inspired algorithms that allows precise control on the sampling of synthetic identities and variations thereof. More precisely, our method treats samples as soft spherical particles, living in the multi-dimensional latent or embedding spaces, subjected to repulsive inter-particles contact forces, a random brownian force as well as a global attractive potential. Due to the similarity of this kind of dynamics to the *Langevin equation*, a stochastic differential equation (SDE) that describes the *Brownian motion* of small particles in a solvent and its generalization, we call our first algorithm *Langevin*. This algorithm allows us to approach a dense packing of the spherical identities while keeping latent space spread minimal and thus filling up the latent space starting by the regions that yield the most realistic images. In addition to *Langevin*, that generates the *inter-class* distributions, we also develop two similar algorithms, called *Dispersion* and *DisCo*, to generate *intra-class* variations, Fig. (1) shows example of images generated with this method. We perform an exploration of the parameter space of these algorithms and generate several synthetic face datasets. We then validate our approach by training FR models with this synthetic data, showing that our method can out-perform the state-of-the-art of previous GAN based models.

This article brings the following contributions to the field

- The *Langevin* algorithm that generates a sampling of synthetic identities within a GAN’s latent space opti-

This research is based upon work supported by CITeR (Center for Identification Technology Research) project LEGAL2 (CITeR-21F-02i-M). This work was also funded by the Hasler foundation through the Responsible Face Recognition (SAFER) project as well as the H2020 TReSPAsS-ETN Marie Skłodowska-Curie early training network (grant agreement 860813).

Authors are with the Biometrics Security and Privacy Group of Idiap Research Institute, Martigny, Switzerland. Hatef Otrosi Shahreza is also affiliated with École Polytechnique Fédérale de Lausanne (EPFL) and Sébastien Marcel is also affiliated with Université de Lausanne (UNIL).



Fig. 1: Example of synthetic faces generated using StyleGAN2. The three rows are three different classes generated with the *Langevin* algorithm while the columns show *intra-class* variations generated using the *Dispersion* algorithm.

mizing *inter-class* distances, based on a loss function inspired by granular materials first used in this field.

- The *Dispersion* and *DisCo* algorithms that generate *intra-class* variations for an ensemble of synthetic identities, based on the same mechanism as well as pre-computed latent directions for the second one.
- A detailed exploration of the parameter space of these algorithms to optimize both the algorithms and synthetic datasets performances, which offer a new view point on the structure of GAN models latent space.
- An investigation on whenever these algorithms can be used to protect privacy by preventing leakage from the training set.

This article is structured as follows: After reviewing the existing literature in section 2, section 3 describes our physics-inspired methods for identity diffusion and generation of synthetic datasets. In section 4 we present experiments that validate our approach and, finally, in 5 we show our conclusions and future work directions.

2 RELATED WORK

2.1 Generative Adversarial Networks

Generative Adversarial Networks (GANs) [18], [19] are unsupervised or semi-supervised models that map high-dimensional data to a smaller latent space. They are typically composed of a pair of networks, the generator and the discriminator, that are trained together in a competitive, i.e. adversarial, fashion. The generator has never access to the real data during training but rather generates its output from a noise signal. The discriminator, on the other hand, has access to both the real data and the output from the

generator. While training, the generator learns to generate data resembling the source dataset using input from the discriminator which concurrently learns to better discriminate between genuine and fake data.

Here we focus our attention on a family of style-based GAN architectures, such as StyleGAN [20], StyleGAN2 [21], StyleGAN3 [22], EG3D [23], etc., that can generate high-resolution and high-quality face images. These networks have the unconventional feature that the input latent vector $z \in \mathcal{Z}$ is first transformed by a *mapping network* to intermediate vector $w \in \mathcal{W}$. The latter is then transformed by affine transformation before being injected in the various layers generator. StyleGAN2 [21] improves normalization and regularization of the original StyleGAN and removes generation artifacts. StyleGAN3 [22] improves the StyleGAN2 architecture by removing dependencies in absolute pixel coordinates by working in frequency space and is better adapted for animations. These network are typically trained on the Flickr-Faces-HQ Dataset (FFHQ) dataset [20] or a 3D texture version of this dataset (FFHQ-UV) [24].

2.2 GAN inversion and editing

For a given generative network, an open question is how to *invert* a given image, i.e. find the latent vector whose generated output is the most similar to to input image. In [25], it was found that it is not easy to embed face images in the latent spaces \mathcal{Z} or \mathcal{W} , using the \mathcal{W}^+ space where inputs of each layers is different yields more robust results. In [26], it is proposed to use a domain-guided encoder trained with real images to keep the semantic structure of the latent space. Other approaches exist, for instance in [27] fine-tuning of the generator hyper-parameters is performed to achieve very accurate results. Similarly, the authors in

TABLE 1: Comparison of the existing synthetic face datasets present in the literature with the best performing datasets created in this work. In addition to the number of identities and number of images, we present the recognition accuracy obtained by training an FR model on each dataset and evaluating on standard face recognition benchmarking datasets. The best value in each category is emboldened and the best results achieved by training from synthetic datasets amongst all categories of synthetic datasets are underlined.

Dataset Type	Dataset name	Generator	N_{id}	$N_{samples}$	LFW	CPLFW	CALFW	CFP	AgeDB
Real images	MS-Celeb-1M [4]	N/A	85'000	5'800'000	99.82	92.83	96.07	96.10	97.82
	WebFace-4M [5]	N/A	206'000	4'000'000	99.78	94.17	95.98	97.14	97.78
	CASIA-WebFace [6]	N/A	10'572	490'623	99.42	90.02	93.43	94.97	94.32
Computer Graphics	DigiFace-1M [7]	Rendered mesh	109'999	1'219'995	90.68	72.55	73.75	79.43	68.43
Diffusion-based	DCFace-0.5M [8]	custom trained	10'000	500'000	98.35	83.12	91.70	88.43	89.50
	DCFace-1.2M [8]	custom trained	60'000	1'200'000	98.90	84.97	92.80	89.04	91.52
	IDiff-Face (Uniform) [9]	custom trained	10'049	502'450	98.18	80.87	90.82	82.96	85.50
	IDiff-Face (Two-Stage) [9]	custom trained	10'050	502'500	98.00	77.77	88.55	82.57	82.35
GAN-based	Synface [10]	StyleGAN2 ^b	10'000	999'994	86.57	65.10	70.08	66.79	59.13
	SFace [11]	StyleGAN2 [#]	10'572	1'885'877	93.65	74.90	80.97	75.36	70.32
	SFace2 [12]	StyleGAN2 [#]	10'572	1'048'255	94.03	73.2	80.33	74.87	72.98
	Syn-Multi-PIE [†] [13]	StyleGAN2	10'000	1'800'000	78.72	60.22	61.83	60.84	54.05
	GANDiffFace [14]	StyleGAN3	10'080	543'893	94.35	76.15	79.90	78.99	69.82
	IDnet [15]	StyleGAN2 [#]	10'577	1'057'200	84.48	68.12	71.42	68.93	62.63
	ExFaceGAN [16]	GAN-Control	10'000	599'944	85.98	66.97	70.00	66.96	57.37
	<i>Langevin-Dispersion</i> [ours]	StyleGAN2	10'000	650'000	94.38	65.75	86.03	65.51	77.30
	<i>Langevin-DisCo</i> [ours]	StyleGAN2	10'000	650'000	97.07	76.73	89.05	79.56	83.38
<i>Langevin-DisCo</i> [ours]	StyleGAN2	30'000	1'650'000	98.97	81.52	93.95	83.77	93.32	

[†] Dataset was re-generated from the original source code [#] Identity conditioned ^b Disentangled representation [17]

[28] introduced Pivotal Tuning Inversion (PTI) where hyper-parameters were fine-tuned around a original latent code.

Given a latent vector, either randomly sampled or from an inverted image, an important question is how to modify it to change some attributes, e.g. pose, while keeping other fixed, especially identity. In a [13], a method using latent inversions of the *Multi-PIE*¹ dataset coupled with a linear Support Vector Machine (SVM) is introduced, allowing to generate identity preserving variations by latent editing, which the authors apply to generate the *Syn-Multi-PIE* synthetic dataset. In [29], a fully connected latent-to-latent network with several loss functions, in particular one that preserves identity, was proposed. In [30], a method based on Higher-Order Singular Value Decomposition (HOSVD) is proposed to edit emotions. Point motion supervised editing is introduced in the DragGAN method [31] which iteratively corrects the latent vector to achieve motion of a set of points in the image plane. High-Fidelity talking-head synthesis (HiDe-NeRF) is introduced in [32] for NeRFs. The authors of [33] present *pix2pix3D*, a 3D-aware conditional generative model capable of photorealistic image synthesis from a 2D label map.

2.3 Diffusion models

Diffusion probabilistic models are another class of generative models that are trained to generate an image from a random noise through a gradual denoising process [34], [35]. In these models, the input image is corrupted by a random Gaussian noise, and then a denoising diffusion network is trained to generate a clean image. Therefore, after training the denoising diffusion network can generate a new image from a random Gaussian noise. In spite of a high visual fidelity in image generation of diffusion models [36], training denoising diffusion models directly in the pixel

space of the image requires large computation resources. In addition, the latent space of diffusion models lacks semantic context, which makes it difficult for representation learning. To address these issues, latent diffusion models were proposed, which consist of a pretrained autoencoder where the image is encoded into the latent space of the autoencoder, and then the probabilistic denoising process is applied in the latent space [37], [38]. Then, given a random noise in the latent space, a new latent code is generated, which is used by the decoder to generate new images. The latent diffusion models also enable conditional image generation and are used for different tasks, such as text-to-image generation, inpainting, etc [36], [37]. However, compared to the latent space of StyleGAN-based models, that includes style-based representation, the style information is not disentangled in the latent space of latent diffusion models, which makes image editing in the latent space a difficult task. To address this issue, several papers proposed conditional models and trained the latent diffusion models with a condition input. For example, in [9] an identity-conditioned diffusion model was proposed to generate different images of one subject using latent diffusion models. In [8], a diffusion model with dual conditions was proposed to generate face images with different styles and different identities.

Despite the recent increase in the application of diffusion models in different tasks, there are some works that show the leakage of training data in diffusion models [39]–[43]. As a matter of fact, in the training of diffusion models, the network is directly optimised to generate training samples through denoising part, and therefore the network directly learns from training data. Such a leakage from the training data in diffusion models creates major concerns for the application of diffusion models in privacy-sensitive problems, such as biometrics.

1. www.cs.cmu.edu/afs/cs/project/PIE/MultiPie/Multi-Pie/Home.html

2.4 3D Modeling

Another avenue for generating synthetic face images is to render a 3D Morphable Models (3DMM) [44]. For instance the Basel Face Model (BFM) [45] has been widely used and provides a parametric 3D shape and texture model from 3D facial scans. A new version of this model [46], based on Gaussian process morphable models was developed more recently. The Faces Learned with an Articulated Model and Expressions (FLAME) model is introduced in [47] with a focus on expressions. In [48] a highly realistic non-linear face model, based on 4000 high resolution scans, yields ultra high definition up to the skin pore level. In [49] a model that extracts realistic mesh-based avatars from a single image is presented. In [50] the authors develop a similar avatar generation technique using differential rendering. The authors of [51] show that it is possible to train face recognition models with rendered face models only. In [52] a model that extracts parameters for the BFM model from a single picture is presented, allowing to find a 3D face model that accurately fits the input face image and its spacial position with respect to the camera.

In addition to rendering approach, recently, a lot of research was focussed on 3D aware generative models, for instance with Neural Radiance Fields (NeRF) [53], which work by sampling location and viewing direction of the light rays and use volume rendering techniques to generate new views from a set of existing pictures of a 3D shape. For example, EG3D [23] extends the StyleGAN2 network by adding a tri-plane-based realistic depth representation in the network allowing a given generated image to be transformed in 3D space.

2.5 Synthetic Dataset and Model Training

Considering the legal and privacy concerns in FR models trained with large real face datasets, several works proposed new synthetic face recognition datasets (composed of different synthetic subjects with several samples per identity) to use for training face recognition models. Table 1 compares the synthetic datasets in the literature, and benchmarks the performance of face recognition models trained with the same backbone² using each dataset.

DigiFace [7] used a computer graphic pipeline to render digital faces and introduce different variations based on face attributes (e.g., variation in facial pose, accessories, and textures). In contrast to DigiFace, other methods used generative neural networks based on GANs or diffusion models. SynFace [10] used a modified StyleGAN2 [17] to generate synthetic images as different identities and then generated different samples by mixing identities in latent space. SFace [11] used CASIA-WebFace [6] to train identity-conditioned StyleGAN and then used it to generate a synthetic dataset. The similar approach was used in SFace2 [12], but instead sampling step was performed in the latent space. GANDiffFace [14] used StyleGAN to generate synthetic identities and then used DreamBooth [54] to generate different samples for each identity. IDnet [15] used a three-player GAN framework to generate a synthetic dataset using the StyleGAN model as a generator, and the third

player is trained to generate identity-separable face images. Syn-Multi-PIE [13] used StyleGAN to generate synthetic face images and then explored the latent space to generate different samples per identity. ExFaceGAN [16] used GAN-based face generator models (such as StyleGAN2 [21], StyleGAN3 [22], or GAN-Control [55]) and learned an identity boundary in the latent space of GAN model. In contrast to most works based on GAN models, recently DCFace [8] and IDiff-Face [9] were proposed which used diffusion models to generate synthetic datasets. As described in section 2.3, in contrast to GAN-based face generator models like StyleGAN, the latent space of diffusion models lack style representation, and therefore DCFace [8] and IDiff-Face [9] trained conditional diffusion models. DCFace [8] used CASIA-WebFace [6] to train a dual condition diffusion model with style and identity conditions. IDiff-Face [9] trained an identity-conditioned diffusion model and used it to generate different samples of each subject.

The results of benchmarking in Table 1 show that our method achieves superior performance compared to GAN-based methods. Compared to diffusion-based datasets, our method outperforms IDiff-Face on all benchmarking datasets and achieves a competitive performance with DCFace. However, we should note that, as mentioned in section 2.3, diffusion models are shown to be prone to leaking information from their training samples [39]–[43], which limits their application in tasks with sensitive data. In fact, the main motivation for generating synthetic datasets is to resolve the privacy concerns in large-scale real face recognition datasets. However, if the generated synthetic dataset has a leakage of information from a real dataset, it will have similar privacy issues. The results in Table 1 also show that there is still a gap between training with synthetic and real face recognition datasets.

3 IDENTITY DIFFUSION AND SYNTHETIC DATA GENERATION

In this work, we focus on GANs generators as their latent space has a tractable dimensionality, even if our approach can be generalized to other types of generative networks. Moreover, we specialize in the StyleGAN family of models as this provides a wide variety of generators that are easily interchangeable.

To generate a random face image on a StyleGAN type network, one first sample a point z from a Gaussian distribution in an auxiliary latent space \mathcal{Z} , then map it to a latent space vector $w \in \mathcal{W}$ using a fully connected mapping network and finally generate an image $i \in \mathcal{I}$ using a generator network $g(w)$. This purely gaussian sampling however yields a distribution of identities that are not sufficiently dissimilar to train an FR model. The following sections present the *Langevin* algorithm that iteratively optimizes an initially random ensemble of synthetic identities towards a more suitable one where identities are distant enough.

In addition to an ensemble of synthetic identities, most FR tasks also require *intra-class* variations, in other terms several samples of the same synthetic identity. As summarized in section 2, several approaches have been proposed in the literature. While several of these approaches could in principle be combined with the *Langevin* algorithm, we

2. Training detail is described in section 4.1.

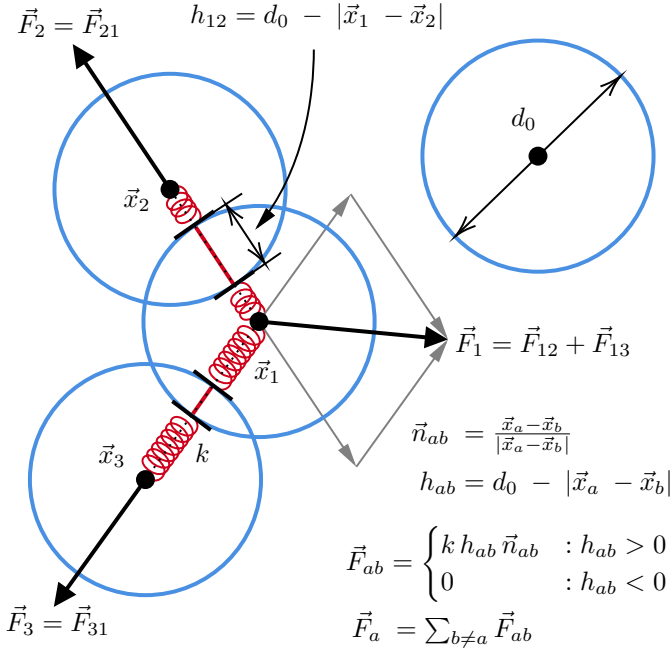


Fig. 2: Simplified model of contact forces between soft spherical bodies. The bodies are characterized by their position \vec{x}_a and diameter d_0 , from which one derives the overlap h_{ab} and a unit vector \vec{n}_{ab} parallel to $\vec{x}_a - \vec{x}_b$. The force exerted on the body a by the body b is denoted \vec{F}_{ab} and the total force on body a by \vec{F}_a .

choose here instead to adapt the latter to produce also *intra-class* variations. This identity *Dispersion* algorithm, for each class, samples the latent space around the identity reference latent vector and optimize this *intra-class* ensemble in a way that samples are close in embeddings space. Finally we present the *DisCo* algorithm which combines identity *Dispersion* with latent directions augmentation pioneered in [13].

3.1 Physics Inspiration

3.1.1 Granular Mechanics

The dynamics of granular assemblies is a fundamental, yet poorly understood, problem in engineering, mathematics and physics. While granular materials are ubiquitous to this world, they exhibit very complex behaviors, such as jamming [56] and spontaneous structure formation [57], that are explained neither by standard thermodynamics nor fluid dynamics.

We take here inspiration from a numerical method for simulating granular assemblies called Discrete Element Method (DEM) [58], where contact interactions are modeled as a spring-like force whose magnitude is proportional to the overlap of the particles Fig. (2). More specifically, each particle is modelled as a perfect sphere of diameter $d_0 = 2r_0$, labelled with indices $a, b, c, \dots = 1 \dots N$, $\vec{x}_a = (x_a^i)$ being the position of the center of the a -th particle in an euclidean D -dimensional space $i, j, \dots = 1 \dots D$. Each particle is allowed to have a small overlap $h_{ab} = d_0 - |\vec{x}_a - \vec{x}_b|$ with its neighbors. While in DEM, an energy dissipating term is

present in the contact force, we consider here a conservative, friction-less, contact force, derived from a quadratic potential

$$V = V(\vec{x}_1, \dots, \vec{x}_N) = \sum_{a=1}^N \sum_{b=a+1}^N V^{\text{cont}}(\vec{x}_a, \vec{x}_b),$$

$$V^{\text{cont}}(\vec{x}_a, \vec{x}_b) = \begin{cases} \frac{k}{2} (d_0 - |\vec{x}_a - \vec{x}_b|)^2 & : |\vec{x}_a - \vec{x}_b| < d_0 \\ 0 & : |\vec{x}_a - \vec{x}_b| > d_0 \end{cases}, \quad (1)$$

where k is the spring constant and $x = \{\vec{x}_1 \dots \vec{x}_N\}$. The sum of the contact forces acting on particle a can be recovered by taking minus³ the gradient w.r.t. the particle's position \vec{x}_a

$$\vec{F}_a = -\vec{\nabla}_{\vec{x}_a} V \quad (2)$$

Instead of a dissipative contact force, we model here energy dissipation with a force in the bulk, proportional to the velocity $\dot{\vec{x}}_a = \frac{d\vec{x}_a}{dt}$, yielding the following Newton equation

$$m\ddot{\vec{x}}_a = -\mu\dot{\vec{x}}_a + \vec{F}_a \quad (3)$$

where m is the mass of the particle, $\ddot{\vec{x}}_a = \frac{d^2\vec{x}_a}{dt^2}$ is the acceleration and μ is the viscous force constant. We note that this loss function is a close relative of non-linear Hinge Losses commonly used in SVM algorithms [59].

3.1.2 Brownian Dynamics

Brownian motion was discovered by botanist Robert Brown while observing the stochastic motion of pollen particle, and explained by Einstein in 1905 by random collision with solvent molecules in one of physics' most famous paper [60]. The effect of the solvent molecules colliding with the particles is modeled by a time-dependent random force $\vec{\Gamma}_a(t)$ which is assumed not to favor any particular direction

$$\langle \vec{\Gamma}_a(t) \rangle = 0. \quad (4)$$

This force is assumed to have a Gaussian probability distribution and is Markovian with the following temperature dependent self-correlation relation

$$\langle \vec{\Gamma}_a(t') (\vec{\Gamma}_b(t))^T \rangle = 2\mu k_B T \mathbb{I}_{D \times D} \delta_{ab} \delta(t' - t), \quad (5)$$

where μ is the viscous coefficient, k_B the Boltzmann constant and where T is the temperature. The dynamical equation for the brownian particles is called the *Langevin* equation and is a Stochastic Differential Equation (SDE) essentially obtained by adding the random force $\vec{\Gamma}_a(t)$ on the right hand side of the Newton equation Eq. (3). In this particular body of work, we are not directly interested by modeling a physical processes, in particular we neglect inertia. While a formal derivation is out of the scope of this work, the resulting dynamical equation simply reads

$$\mu\dot{\vec{x}}_a = \vec{F}_a + \vec{\Gamma}_a(t). \quad (6)$$

The curious reader is referred for instance to [61], [62] for a more formal treatment of such kind of equations.

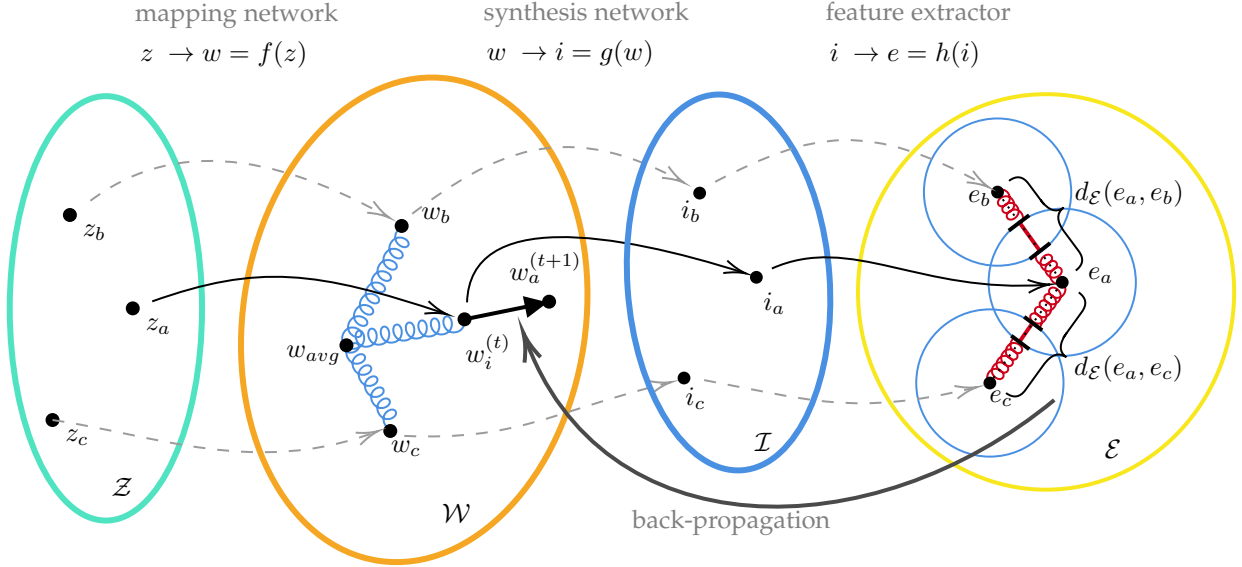


Fig. 3: Mappings between the different spaces and details of the *Langevin* algorithm. Firstly, a random vector z_a is sampled from a normal distribution in \mathcal{Z} , for each identity class $a = 1 \dots N_{id}$. It is then mapped to the initial latent $w_a^{(0)} \in \mathcal{W}$ via the *mapping network* f . A face image is generated from this latent using the generator *synthesis network* $i_a = g(w_a)$ and, after face alignment, the face embedding is computed with the reference *feature extractor* $e_a = h(i_a)$. Two quadratic loss functions are introduced, one on the embedding space \mathcal{E} , depending on the embedding distance $d^{\mathcal{E}}$, and one on the latent space \mathcal{W} distances $d^{\mathcal{W}}$. Their derivatives are evaluated using back-propagation and the latents are updated based on these gradients $w_a^{(t)} \rightarrow w_a^{(t+1)}$. The procedure is repeated for a desired number of iterations N_{iter} .

3.2 Identity Embeddings and Metrics

We consider a generative model $g(w)$ that maps a latent space \mathcal{W} to an image space \mathcal{I} Fig. (3). In the case of the StyleGAN family of models, this network is complemented by a mapping network $f(z)$ that maps an auxiliary space \mathcal{Z} where gaussian sampling is performed. In addition to this generative model, we select an off-the-shelf face recognition (FR) model $h(i)$ that extracts a face embedding vector $e \in \mathcal{E}$. To obtain an embedding from a random latent sample, one evaluates the following chain

$$\begin{aligned} z_a &\sim \mathcal{N}(1, \mathbb{I}), \\ w_a &= f(z_a), \\ i_a &= g(w_a), \\ e_a &= h(i_a). \end{aligned} \quad (7)$$

The FR models we select in this work are all based on the ArcFace loss function [63], which has a spherical symmetry. To be consistent with this loss function, we define an angular metric on the embedding space \mathcal{E} that simply measure the angle between the vectors

$$d^{\mathcal{E}}(e_a, e_b) = \arccos \frac{e_a \cdot e_b}{|e_a| |e_b|}. \quad (8)$$

This in turns allows us to put a identity aware metric on the latent space

$$d_{id}^{\mathcal{W}}(w_a, w_b) = d^{\mathcal{E}}(e(w_a), e(w_b)) \quad (9)$$

where $e(w) = h(g(w))$.

3. The minus sign is a common convention in physics.

3.3 Identity Sampling and Inter-Class Optimization

3.3.1 Random-Reject Sampling Algorithm

We first consider a simple identity sampling algorithm as a baseline. This algorithm works iteratively by randomly sampling a latent vector w_{n+1} and then computing its face embedding e_{n+1} . It then compute the distances $d^{\mathcal{E}}$ between e_{n+1} and the n previously accepted samples $\{e_a, a = 1 \dots n\}$ and, if all these values are above an Inter-Class Threshold (ICT), the sample w_{n+1} is itself accepted. If not the procedure is repeated until a sample that satisfies this criterion is found. This process is repeated until the desired number of identities N_{id} is reached. This algorithm, used for instance in [13], while perfectly suitable to find sufficiently dissimilar identities, unfortunately scales exponentially with the number of identities making it hard to apply to large datasets. We call this algorithm *Reject* in following sections.

3.3.2 Identity Sampling from Langevin Dynamics

To circumvent the scaling problem of the aforementioned *Reject* sampling algorithm, we present here an iterative algorithm, inspired by the physical systems presented earlier in this section. The main idea is to introduce a *repulsive force* between the embeddings $e_a = e(w_a)$ so that they naturally arrange themselves in an assembly that maximize their inter-class distances. While any kind of repulsive force, found in the physical world or not, could in principle serve this purpose, a spring-like force that has a linear dependency on the position seems the simplest choice. Moreover, such type of forces are independent of the dimensionality of the space they act in. On the contrary, other physical forces such as

gravity or electrostatics are described by power laws with exponents that depends crucially on the dimensionality of space and seem less adapted for our purpose.

Ideally, we do not want that identities that are far away interact together, only identities pairs whose distance is below a certain ICT value should lead to a repulsive force. With this criterions in mind, we observe that the potential for non-dissipative granular contact interactions in Eq. (1) achieves precisely this, as the interaction vanishes when the distance is bigger than a constant d_0 . Based on these ideas, we define the identity granular repulsion loss

$$\mathcal{L}^{\mathcal{E}} = \frac{k^{\mathcal{E}}}{2} \sum_{a=1}^{N_{id}} \sum_{b=a+1}^{N_{id}} \begin{cases} (d_0 - d_{ab}^{\mathcal{E}})^2 & : d_{ab}^{\mathcal{E}} < d_0 \\ 0 & : d_{ab}^{\mathcal{E}} > d_0 \end{cases} \quad (10)$$

$$d_{ab}^{\mathcal{E}} = d^{\mathcal{E}}(e(w_a), e(w_b)) = d_{id}^{\mathcal{W}}(w_a, w_b).$$

Sampling a set identities that satisfy a minimal distance threshold is similar to a sphere packing problem. While solutions to this problem are known for two and three dimensions, higher dimensional optimal sphere packings are usually unknown, except in some special cases [64]. Ideally, we would like our algorithm to generate the densest packing possible to get the most identities from a given generative network. In practice however, at least in low dimensionality, granular materials tend to immobilize in *jammed states* where particle are inter-locked in a way that can block further rearrangement of the granular elements. Both common intuition and advanced engineering practices suggest to add vibrations to the system to avoid such problems. While it is unclear that jamming can be problematic in our high dimensional setup, we nevertheless introduce a random force similar to the one driving Brownian motion described earlier in this section and parametrized by a constant η_0 , and which is linked to the temperature via Eq. (5). While a-priori unrelated, jamming transitions have already been studied in the context of loss landscapes of deep neural networks [65].

Generative models, and GANs in particular, generate good quality images when the input latent vector is in a subspace of the full latent space. For instance, the StyleGAN family of models implements the so-called *truncation trick* which consists by rescaling the latent vector by a constant factor w.r.t. an origin placed at the average latent w_{avg} calculated by sampling a large number of vectors via the mapping network. In other words, the best quality images are those with latents located near w_{avg} . Introducing purely repulsive interactions alone would be problematic as the latent vectors would be pushed away from the domain where the network generates the best quality data. To circumvent this we introduce a latent pull-back loss function, quadratic as well, that keeps the identities from wandering too far from the w_{avg} latent

$$\mathcal{L}^{\mathcal{W}} = \frac{k^{\mathcal{W}}}{2} \sum_{a=1}^{N_{id}} |w_a - w_{avg}|^2 \quad (11)$$

We call the resulting identity sampling algorithm *Langevin* due to its similarities with the equations describing motion a small soft particles in a thermal bath.

3.3.3 Numerical Implementation

As said earlier we focus on the case where viscosity is dominant w.r.t inertia. For physical particles we thus need to solve the first order stochastic differential equation in Eq. (6), which we approximate by

$$\begin{aligned} \vec{x}_a(t + \delta t) &\approx \vec{x}_i(t) + \frac{\delta t}{\mu} \vec{F}_a + \frac{\eta_0}{\mu} d\vec{W}(t, \delta t) \\ &= \vec{x}_i(t) - \frac{\delta t}{2} \frac{k}{\mu} \vec{\nabla}_{\vec{x}_a} \sum_{a,b>a} h_{ab}^2 + \frac{\eta_0}{\mu} d\vec{W}(t, \delta t) \end{aligned} \quad (12)$$

where we see that the viscosity constant μ scales the other constants k and η_0 . For the following discussion we set the viscosity to be $\mu = 1$ and use the other constants to parametrize the problem. Our latent update algorithm, inspired by the above simple numerical scheme, reads:

$$w_a^{(t+1)} = w_a^{(t)} - \delta t \nabla_{w_a} \mathcal{L}^{(t)} + \eta_0 \sqrt{\delta t} \zeta_a^{(t)}, \quad (13)$$

where $\zeta_a^{(t)}$ is a vector of independent normal variables of variance $\sigma = 1$ and where

$$\mathcal{L}^{(t)} = \left(\mathcal{L}^{\mathcal{E}} + \mathcal{L}^{\mathcal{W}} \right) \left(w_1^{(t)}, \dots, w_N^{(t)} \right). \quad (14)$$

From a numerical perspective, the gradient of $\mathcal{L}^{\mathcal{W}}$ can be easily calculated so the only challenging task is the computation of the gradient of the embedding distance metric $\nabla_a d_{bc}^{\mathcal{E}}$. This computation can be challenging because the embedding computation passes through two networks, the generator and the embedding extractor, and through a very high dimensional image space. One can simplify the problem by computing the jacobian $\frac{\partial e}{\partial w}$, but it is still quite computationally expensive. We find that a more efficient way of performing this computation is to first compute all the embeddings with a forward only pass, and then compute the gradients in a second pass. This procedure allows us to make the problem tractable on standard computing hardware, even for a large number of identities. We still need to determine a appropriate time-step for our calculations. We will show in the next section that the time-step has little impact, a wide range of values yielding acceptable performance. Values too coarse can however lead to numerical problems that can have a negative impact over the quality of the resulting dataset. Looking at Eq. (13), and neglecting the random force, we see that the maximal distance a latent can move in a single time-step, $\arg \max |w_a^{(t+1)} - w_a^{(t)}|$ is proportional to the time-step times $\arg \max |\nabla \mathcal{L}^{(t)}|$. If we impose that this distance should remain smaller than a proportion $\tau < 1$ of the minimal latent-to-latent distance, we find the following expression for the time-step

$$\delta t = \tau \frac{\arg \min |w_a - w_b|}{\arg \max |\nabla \mathcal{L}^{(t)}|}, \quad (15)$$

which prevent latents to be updated too aggressively while still giving good numerical performance when the distribution is close to an equilibrium. The final *Langevin* algorithm is depicted in Algorithm 1.

3.4 Within Identity Sampling and Intra-Class Variations

3.4.1 Identity Dispersion

As we are interested in generating synthetic datasets that can be used to train FR models, we need variations of

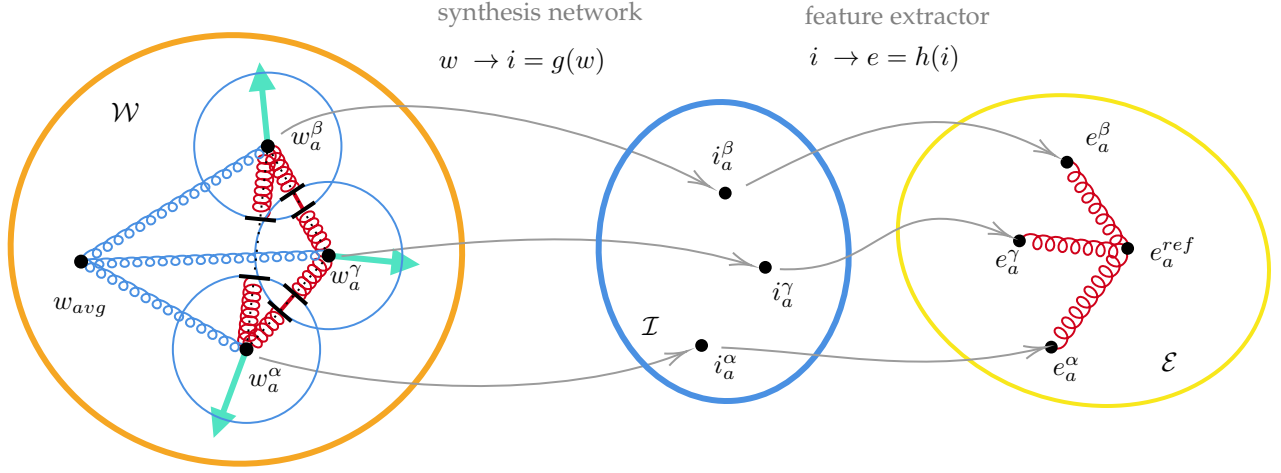


Fig. 4: The *Dispersion* algorithm is quite similar to *Langevin*, with slightly different loss functions, and is intended to generate N_{var} intra-class variations per identity class. In a first step, for each variation $\alpha = 1 \dots N_{var}$, a latent vector $w_a^{\alpha(0)}$ is initialized from its reference value w_a^{ref} plus some noise. Three loss function are then computed. The first one acts on the embedding space and pulls the embeddings of the variations towards the reference embedding e_a^{ref} . The second loss function act on the latent space and pulls the latent vectors towards the average latent w_{avg} . The last one is a granular loss function that exert a repulsive force between latent vectors that are closer than a certain threshold. Latent vectors are updated according to the gradients of these losses. The procedure is repeated for each class $a = 1 \dots N_{id}$ and for a desired number of iterations N_{iter}^{disp} .

Algorithm 1 Langevin algorithm

```

1: for  $a = 1 \dots N_{id}$  do
2:    $z_a \leftarrow \mathcal{N}$ 
3:    $w_a \leftarrow f(z_a)$ 
4: end for
5: for  $N_{iter}$  do
6:   for  $a = 1 \dots N_{id}$  do
7:      $i_a \leftarrow g(w_a)$ 
8:      $e_a^{cst} \leftarrow h(i_a)$ 
9:   end for
10:  for  $a = 1 \dots N_{id}$  do
11:     $i_a \leftarrow g(w_a)$ 
12:     $e_a \leftarrow h(i_a)$ 
13:     $d_{ab}^{\mathcal{E}} \leftarrow d^{\mathcal{E}}(e_a, e_b^{cst}), b \neq a$ 
14:     $f_a \leftarrow -\nabla_a (\mathcal{L}^{\mathcal{E}} + \mathcal{L}^{\mathcal{W}})$ 
15:  end for
16:   $f^+ \leftarrow \arg \max f_a$ 
17:   $\delta w^- \leftarrow \arg \min |w_a - w_b|$ 
18:   $\delta t \leftarrow \tau \delta w^- / f^+$ 
19:  for  $a = 1 \dots N_{id}$  do
20:     $\zeta_a \leftarrow \mathcal{N}$ 
21:     $w_a \leftarrow w_a + \delta t f_a + \sqrt{\delta t} \zeta_a$ 
22:  end for
23: end for
  
```

the synthetic identities, so called within-class variations. We devise here a second algorithm, called *Dispersion*, that generates an arbitrary number of variations from a reference latent-embedding pair (w_a^{ref}, e_a^{ref}) while preserving as much as possible the identity. This algorithms, depicted in Fig. (4), is very similar to the previous *Langevin* algorithm and is intended to be used to after a suitable set of identities have been generated by the latter. Given a number N_{id} of

references identities, this algorithm creates N_{var} variations w_a^{α} , with $\alpha = 1 \dots N_{var}$. To keep these new latent vectors separated enough, to create variability, we introduce another granular loss function, but this time in the latent space

$$\mathcal{L}_{disp}^{\mathcal{W}} = \frac{k_{disp}^{\mathcal{W}}}{2} \sum_{a=1}^{N_{id}} \sum_{\alpha=1}^{N_{var}} \sum_{\beta=\alpha+1}^{N_{var}} \begin{cases} (d_0^{\mathcal{W}} - |w_a^{\alpha} - w_a^{\beta}|)^2 & : |w_a^{\alpha} - w_a^{\beta}| < d_0^{\mathcal{W}} \\ 0 & : |w_a^{\alpha} - w_a^{\beta}| > d_0^{\mathcal{W}} \end{cases} \quad (16)$$

For the present work, we do not compute contact forces between different identities for identity variations, even if this could potentially improve performance. This is done mainly for simplicity reasons as such extension would require parallelization with custom inter-GPU communications. To keep the embeddings of the identities variations close to the reference embedding, we introduce a further spring-like quadratic loss function

$$\mathcal{L}_{disp}^{\mathcal{E}} = \frac{k_{disp}^{\mathcal{E}}}{2} \sum_{a=1}^{N_{id}} \sum_{\alpha=1}^{N_{var}} d^{\mathcal{E}}(e(w_a^{\alpha}), e_a^{ref})^2, \quad (17)$$

which is computed similarly to the granular loss of the *Langevin* algorithm. Finally, we also add the latent pull-back loss in Eq. (11), the total *Dispersion* loss reads

$$\mathcal{L}_{disp} = \mathcal{L}_{disp}^{\mathcal{W}} + \mathcal{L}_{disp}^{\mathcal{E}} + \mathcal{L}^{\mathcal{W}}. \quad (18)$$

The numerical implementation of this algorithm is very similar to the *Langevin* one, the latent update equation simply reads

$$w_a^{\alpha(t+1)} = w_a^{\alpha(t)} - \delta t \nabla_{w_a^{\alpha}} \mathcal{L}_{disp}^{(t)} + \eta_0 \sqrt{\delta t} \zeta_a^{\alpha(t)}. \quad (19)$$

In this article we keep a fixed time-step for *Dispersion*, for simplicity reasons, and parallelize over identities. We initialize the new latents w_a^α with the value of the reference one w_a^{ref} and add some random gaussian noise to break the symmetry of the ensemble

$$w_a^{\alpha(0)} = w_a^{ref} + \xi_0 \xi_a^\alpha, \quad (20)$$

where ξ_a^α is a vector of independent normal variables of variance $\sigma = 1$ and ξ_0 is a fixed scaling parameter.

3.4.2 Latent Editing: Covariates

While the *Dispersion* algorithm creates realistic variations of a given identity, it gives little control over the type of variation created. Moreover, having an alternative method to create variations is desirable to give a comparison point. For this reason we reproduce the latent editing method introduced in [13]. This latent editing technique assumes that the variation of some attribute, such as left-right pose, is essentially a translation in latent space and that this translation is the same for every identity.

Given this assumption and following [13], we project in the latent space the samples of the CMU Multi-PIE face database. This dataset provides a reasonable number of genuine identities, each captured with different poses, illuminations and expressions. When this is done, we use a linear SVM model to fit the latent directions corresponding to the different attributes variations present in the database. In particular, we extract 7 vectors w_I^{cov} corresponding to left-right poses, left-right illuminations and 5 facial expressions: smile, surprise, squint, disgust and scream. The algorithm introduced in [13] based on these latent direction is called *Covariates* in this work and yields a total of 17 variations: 6 different poses, 6 different illuminations and one for each of the 5 expressions.

3.4.3 Combining Dispersion and Covariates (DisCo)

We also propose to combine the *Dispersion* and *Covariates* methods and name the resulting algorithm *DisCo*. The essential difference with the original *Dispersion* algorithm is in the initialization procedure. In addition to the initial symmetry breaking gaussian noise ξ_a^α , the *DisCo* algorithm also adds a linear combination of the 7 *Covariates* vectors w_I^{cov} to the reference latents w_a^{ref}

$$w_a^{\alpha(0)} = w_a^{ref} + \xi_0 \xi_a^\alpha + \sum_{I=1}^7 \lambda_{aI}^\alpha w_I^{cov}, \quad (21)$$

where weights $\lambda_{aI}^\alpha \in [-\lambda_0, \lambda_0]$ are randomly and uniformly sampled in a seven-dimensional hypercube. This additional step forces more intra-class variability at the initial step of the *Dispersion* algorithm and yields, according to our experiments, better performing datasets. This positive effect might be explained by the number of identities variations compared to the dimensionality of the intra-class latent subspace. In the case where the former is small compared to the latter, this extra initialization step helps the latent granular contact loss to spread the latent vectors across the intra-class subspace, yielding a more diverse final dataset.

TABLE 2: Hyperparameters for the *Langevin*, *Dispersion* and *DisCo* algorithms and their default values.

	Default	Description
μ	1.0	<i>Langevin</i> and <i>Dispersion</i> bulk viscosity
$k^\mathcal{E}$	1.0	<i>Langevin</i> embedding contact force coefficient
$d_0^\mathcal{E}$	1.4	<i>Langevin</i> embedding distance threshold
$k^\mathcal{W}$	0.1	<i>Langevin</i> latent pull-back coefficient
η_0	0.01	<i>Langevin</i> random force magnitude
τ	0.3	<i>Langevin</i> variable time-step coefficient
N_{iter}	100	<i>Langevin</i> number of iterations
$k_{disp}^\mathcal{W}$	1.0	<i>Dispersion</i> latent contact force coefficient
$d_0^\mathcal{W}$	12.0	<i>Dispersion</i> latent distance threshold
$k_{disp}^\mathcal{E}$	1.0	<i>Dispersion</i> identity pull-back coefficient
$\tilde{k}^\mathcal{W}$	1.0	<i>Dispersion</i> latent pull-back coefficient
$\tilde{\eta}_0$	0.01	<i>Dispersion</i> random force magnitude
$\tilde{\delta}t$	0.05	<i>Dispersion</i> fixed time-step
\tilde{N}_{iter}	20	<i>Dispersion</i> number of iterations
ξ_0	0.2	<i>Dispersion</i> initial symmetry breaking noise
λ_0	1.0	<i>DisCo</i> covariates sampling scale

4 EXPERIMENTS

In this section we run a series of experiments to demonstrate the validity of our approach and explore, at least partially, the parameter space opened by the algorithms presented above. First, in section 4.1 we describe our experimental setup used in our evaluations, and then we present different experiments to investigate the performance of our synthetic datasets in the remaining sections.

4.1 Experimental Setup

Comparing the quality of synthetic datasets is a challenging endeavor in its own right. While various quality metrics exist, their respective reliabilities have been discussed in the literature and seem far from ideal for our present purpose. We instead choose to train FR models on the data we generate, and then benchmark the resulting models on well-known face biometrics datasets. While computationally expensive this evaluation technique yields relatively reliable and trustworthy results that are easily compared to existing baselines.

4.1.1 Training and Benchmarking

We use the synthetic dataset and train a face recognition model with the iResNet50 backbone using AdaFace loss function [66]. We train each model for 30 epochs using the Stochastic Gradient Descent (SGD) optimizer with the initial learning rate 0.1 and weight decay 5×10^{-4} . Then, we evaluate the performance of the trained models on different benchmarking datasets, including Labeled Faces in the Wild (LFW) [67], Cross-age LFW (CA-LFW) [68], CrossPose LFW (CP-LFW) [69], Celebrities in Frontal-Profile in the Wild (CFP-FP) [70], AgeDB-30 [71], IARPA Janus Benchmark-B (IJB-B) [72] and IARPA Janus Benchmark-B (IJB-C) [73] datasets. To maintain consistency with prior works, the results reported for LFW, CA-LFW, CP-LFW, CFP-FP, and AgeDB datasets are accuracy calculated using

10-fold cross-validation, where the comparison threshold is set at the Equal Error Rate (ERR) on one fold and the accuracy is measured on the remaining folds. In contrast, the standardized approach for reporting results for IJB-B and IJB-C datasets is to find True Match Rate (TMR) at different False Match Rate (FMR) values, and therefore we report Receiver Operating Characteristic (ROC) for evaluating FR models on these two benchmark datasets. For space and formatting reasons, some benchmarks are omitted.

4.1.2 Different Hyperparameters

Our new method introduces a number of hyperparameters that influence the quality and usefulness of the final synthetic datasets. While this gives new opportunities to "tune" a synthetic dataset towards a particular goal, it also adds a new layer of complexity that requires a good understanding of the influence of each of these numbers on the final results. Table (2) shows the list of hyperparameters of the *Langevin*, *Dispersion* and *DisCo* algorithms as well as their default values. These default values give a baseline with good numerical performance and are used in the following experiments unless explicitly specified. To better understand the impact of these hyperparameters, we run a non-exhaustive survey with different values and evaluate the resulting datasets.

4.1.3 Reference FR Backbone

To compute embedding distances and optimize the identity distribution with respect to the latter, we choose an off-the-shelf reference FR model. This model is built on an iResNet50 backbone, with an Arcface loss [63] and trained on the now discontinued *MS-Celeb-1M* dataset [4]. It is part of the software package *bob* [74].

4.2 Dynamical Evolution of *Langevin* Ensembles

The *Langevin* algorithm presented in the previous section is designed to maximize, iteratively and stochastically, the pairwise embedding distances of an ensemble of synthetic identities defined on the latent space of a given generative model. This is achieved using the loss function, Eq. (10), that yields a repulsive force between two samples whose embeddings are closer than a threshold value $d_0^\mathcal{E}$. At the same time, a second loss function, Eq. (11), pulls the samples towards the average latent vector w_{avg} around which the best quality samples are located.

By design, the *Langevin* algorithm tries to increase the samples embedding pairwise distances $d^\mathcal{E}(e_a, e_b)$, up to a given threshold $d_0^\mathcal{E}$, while simultaneously pulling the samples towards w_{avg} , and therefore minimizing pairwise latent distances $|w_a - w_b|$. Fig. (5a) and Fig. (5b) show the evolution of average pairwise embedding and latent distances, respectively, for $N_{id} = 10k$ identities, up to $N_{iter} = 50$ iterations and for five different values of $d_0^\mathcal{E}$. Fig. (5a) shows that all five ensembles start with the same average pairwise embedding distance $\langle d^\mathcal{E} \rangle \simeq 1.47$, this quantity increase very quickly to reach a plateau after approximately 10 time-steps. As expected, bigger values of $d_0^\mathcal{E}$ lead to higher plateaux, with the exception of $d_0^\mathcal{E} = 1.6$ where some sort of saturation phenomenon seems to occur. While average the embedding distance stays almost constant after this swift onset, the

average pairwise latent distance $\langle |w_a - w_b| \rangle$ continue to decrease at a much slower pace, as seen in Fig. (5b), indicating that the ensemble slowly clusters itself around w_{avg} .

These dynamics are driven by the balance between the repulsive embedding contact force, whose evolution is shown in Fig. (5c), and the attractive latent pull-back force, whose evolution is shown in Fig. (5d). We see that, when the samples are randomly distributed, their overlap in embedding space is quite significant leading to very high contact forces in the first iterations. The samples rearrange themselves to minimize contact interactions quite rapidly and, after a certain number of iterations, the contact interaction reaches a plateau. After this plateau is reached, samples continue to be pulled towards w_{avg} by the latent pull-back force, which slowly decays as seen Fig. (5d). Fig. (5e) and Fig. (5f) show this decay for a varying number of identities, by plotting $\langle |w_a - w_b| \rangle$ in function of N_{id} and N_{iter} , respectively.

4.3 Strict Inter-Class Threshold Constraints

Another interesting metric on the performance of the algorithm is the proportion of pairwise distances that are above a certain *inter-class threshold* $d_{ict}^\mathcal{E}$. This can be computed by counting each occurrence where this condition is met, for each possible pair of identities (a, b)

$$\rho_{ict} = \frac{|\{d^\mathcal{E}(e_a, e_b) < d_{ict}^\mathcal{E}, \forall(a, b), a > b\}|}{N_{pairs}}, \quad (22)$$

where we set $a > b$ to avoid double counting and where $N_{pairs} = \frac{N_{id}(N_{id}-1)}{2}$ is the number of possible pairwise interactions. If we set this threshold equal to the *Langevin* repulsion distance threshold, $d_{ict}^\mathcal{E} = d_0^\mathcal{E}$, we can evaluate the ratio of the number of contacts over the number of pairs

$$\rho_0 = \frac{|\{d^\mathcal{E}(e_a, e_b) < d_0^\mathcal{E}, \forall(a, b), a > b\}|}{N_{pairs}} = \frac{N_{contacts}}{N_{pairs}}. \quad (23)$$

Fig. (5g) shows the dynamical evolution of this quantity after a certain number of iterations N_{iter} , for different values of $d_0^\mathcal{E}$. We see that for very high values of $d_0^\mathcal{E}$, this value is close to one so almost every identity is in contact with every other one. For other values we can compute the average number of contacts per identity

$$\frac{2 N_{contacts}}{N_{id}} = \frac{2 \rho_0 N_{pairs}}{N_{id}} = 2\rho_0 (N_{id} - 1), \quad (24)$$

where we have added a factor of two to account for each identity in the pair in contact. We see in Fig. (5g) that, for $d_0^\mathcal{E} = 1.4$ and $N_{id} = 10k$, this ratio stabilizes around $\rho = 0.03$ meaning that each identity is on average in contact with approximately 300 other classes. More generally, the ratio ρ_{ict} is the FMR of the reference FR backbone evaluated on the synthetic dataset and the *Langevin* algorithm tends to iteratively decrease this value until it reaches a plateau.

It would be interesting to know the maximal number of identities N_{id}^{strict} , which satisfy the constraint $d_0^\mathcal{E} > d_{ict}^\mathcal{E}$, we can extract from a given *Langevin* ensemble. For this purpose, we devise a simple *erosion* algorithm that iteratively removes identities from the ensemble until the constraint is satisfied for all pairs of remaining identities. This naive algorithm removes the identities with the maximal number

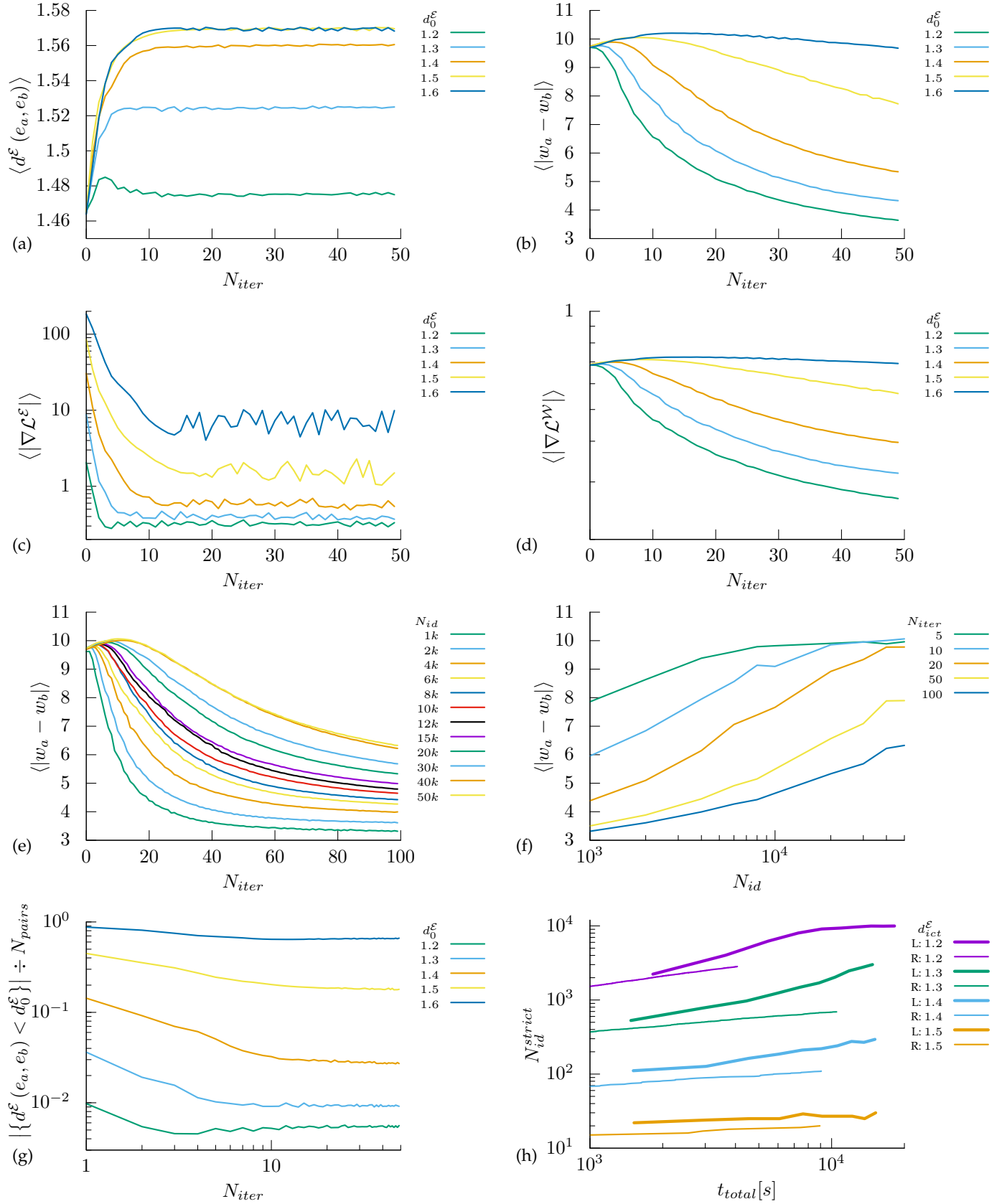


Fig. 5: Dynamics of Langevin ensembles: Evolution of the average pairwise embedding distance (a) and the average pairwise latent distance (b). Evolution of the average embedding contact force (c) and average latent pull-back force (d). Average pairwise latent distance for different N_{id} (e) and pairwise latent distance for N_{id} identities after N_{iter} iterations (f). Proportion of pairwise embedding distances below the threshold $d_0^{\mathcal{E}}$ for $N = 10k$ identities (g). Compute time used to generate N_{id}^{strict} dissimilar identities for Langevin (L) with erosion and for Reject (R) and with different $d_{ict}^{\mathcal{E}}$ values (h).

TABLE 3: Influence of the number of *Langevin* iterations N_{iter} on FR accuracy. For all datasets, variations are created via the *Dispersion* algorithm with default parameters. The first row consider pure random sampling for benchmarking. The next rows show different combination of N_{iter} and $d_0^\mathcal{E}$.

N_{iter}	$d_0^\mathcal{E}$	LFW	CPLFW	CALFW	CFP	AgeDB	Average
0	-	90.78	62.55	78.5	64.96	70.12	73.38
1	1.54	90.73	64.15	78.5	65.24	70.67	73.86
10	1.54	92.23	65.05	81.42	65.5	72.73	75.39
20	1.54	92.73	66.37	82.42	65.09	74.22	76.17
50	1.54	93.93	66.83	84.52	68.67	75.52	77.89
50	1.4	94.45	65.58	86.03	66.53	77.17	77.95
100	1.4	94.72	64.58	86.17	65.36	79.25	78.02

TABLE 4: Influence of *Langevin* time-step parameters on final FR accuracy. The parameter δt is the fixed time-step value while τ is the automatic time-step parameter.

δt	τ	N_{iter}	LFW	CPLFW	CALFW	CFP	AgeDB	Average
0.1	-	200	84.3	56.63	72.33	57.49	65.63	67.28
0.3	-	66	84.12	57.27	71.15	58.63	64.98	67.23
0.6	-	33	83.05	57.65	69.75	57.91	63.7	66.41
1.0	-	20	82.9	57.7	69.9	57.4	61.23	65.83
-	0.3	50	84.12	59.03	72.18	57.8	63.83	67.39
-	1.0	50	82.83	57.73	70.67	58.41	63.57	66.64

of contacts first, one by one, until no contact is left. Fig. (5h) shows values of N_{id}^{strict} for *Langevin* ensembles of $N_{id} = 10k$ and for different values of $d_{ict}^\mathcal{E}$. In this case, we set the contact distance threshold slightly bigger that the threshold, $d_0^\mathcal{E} = 1.1 d_{ict}^\mathcal{E}$, and plot N_{id}^{strict} against computational wall-time. For comparison, we also plot the performance of the *Reject* algorithm and see that *Langevin* with erosion yields a significant numerical advantage, at least with our implementations.

4.4 Performance of the Langevin Algorithms

We are interested in the influence of the number of *Langevin* iterations on the quality of the resulting datasets and, importantly, if the latter improve FR accuracy when compared to random sampling. Table (3) shows the accuracy of FR models trained on synthetic datasets generated with such a varying number of iterations and for two values of $d_0^\mathcal{E}$. The datasets in this table are composed of $N = 10k$ synthetic identities, the first one being the random sampling benchmark. For all datasets, the 64 variations are created with the *Dispersion* algorithm with the standard parameters of Table (2). It is clear that the *Langevin* algorithm yields a significant performance improvement, even after a small number of iterations, over pure random sampling. It is interesting that more iterations tend to yield better performance and that this improvement effect continues even while the average embedding distance has reached a plateau.

While the *Langevin* algorithm seems to yields a significant accuracy advantage for synthetic data trained FR models, it is quite computationally expensive. A straightforward parameter to optimize is the time-step value, which control the precision of the numerical integration. Table (4) shows the effect of the time-step on the final FR accuracy and shows a comparison of fixed time-step against the automatically calculated values. A small advantage is observed for smaller fixed values, at least until $\delta t = 0.3$, and calculated values with $\tau = 0.3$ reach similar performance with slightly

TABLE 5: Influence of the stochastic force on FR accuracy.

η_0	N_{iter}	LFW	CPLFW	CALFW	CFP	AgeDB	Average
0.003	100	94.9	65.4	86.63	65.9	79.35	78.44
0.01	100	94.72	64.58	86.17	65.36	79.25	78.02
0.03	100	94.53	65.67	85.72	64.99	79.22	78.03

less iterations. For this reason, a varying time-step with $\tau = 0.3$ is used in the rest of the article.

Finally, we briefly study the impact of the amplitude of the random stochastic force on the resulting FR performance. The addition of this term was motivated in section 3 by the idea that it could mitigate potential jamming and help sampling the latent space efficiently. Table (5) shows a very limited survey for this purpose, with three different values of η_0 . This data shows that this parameter, at least in this very limited range, has a limited impact on the results. We plan to conduct a more thorough investigation on the stochastic dynamics of these systems in a subsequent publication.

4.5 Repulsion Distances Threshold and *DisCo*

We are now interested in optimizing the statistics of the synthetic datasets generated by our algorithms. In particular, we study here the influence of the repulsion distance thresholds $d_0^\mathcal{E}$ and $d_0^{\mathcal{V}}$, for *Langevin* and *Dispersion*, respectively. We would also like to investigate the impact of the *DisCo* scale parameters λ_0 .

As explained in section 3, the *Langevin* and *Dispersion* granular-like losses functions introduced in Eq. (10) and Eq. (16), respectively, are designed to repulse samples that are too close in the embedding and latent spaces. The *Langevin* algorithm therefore controls the *inter-class embedding pairwise distances* via the parameter $d_0^\mathcal{E}$ as illustrated by the histograms Fig. (6a). One clearly sees that increasing the value of $d_0^\mathcal{E}$ shifts the peak of the distribution toward bigger pairwise embedding distances. For the largest values showed in this plot the peaks are near $d^\mathcal{E} \approx \frac{\pi}{2}$, similar to the real-world data shown in Fig. (6c).

Similarly to *Langevin*, the *Dispersion* algorithm controls the *intra-class latent pairwise distances* via the parameter $d_0^{\mathcal{V}}$. Since increasingly larger latent pairwise distances tend to produce increasingly dissimilar images, we expect bigger values of $d_0^{\mathcal{V}}$ to widen the *intra-class pairwise embedding distances* distribution and shift its peak towards larger values. This is indeed what we observe in the histograms in Fig. (6b), where the *pairwise embedding distances* distributions of *Dispersion* ensembles, created with a wide range of value of the parameter $d_0^{\mathcal{V}}$, are shown. We observe that a small value of $d_0^{\mathcal{V}} = 8.0$ lead to a very narrow distribution, while bigger values greatly shift the peak towards larger $d^\mathcal{E}$ values.

TABLE 6: Influence of *Langevin* repulsion distance threshold $d_0^\mathcal{E}$ on FR accuracy.

$d_0^\mathcal{E}$	N_{iter}	LFW	CPLFW	CALFW	CFP	AgeDB	Average
1.2	50	90.82	59.73	80.97	60.66	72.65	72.97
1.3	50	92.78	63.32	83.33	63.51	74.37	75.46
1.4	50	94.43	65.08	85.13	65.6	76.97	77.44
1.5	50	94.67	65.98	85.1	67.83	75.67	77.85
1.6	50	92.73	65.15	82.28	67.3	73.02	76.10

We are interested on the accuracy of the FR models trained on such synthetic ensembles, for different values of

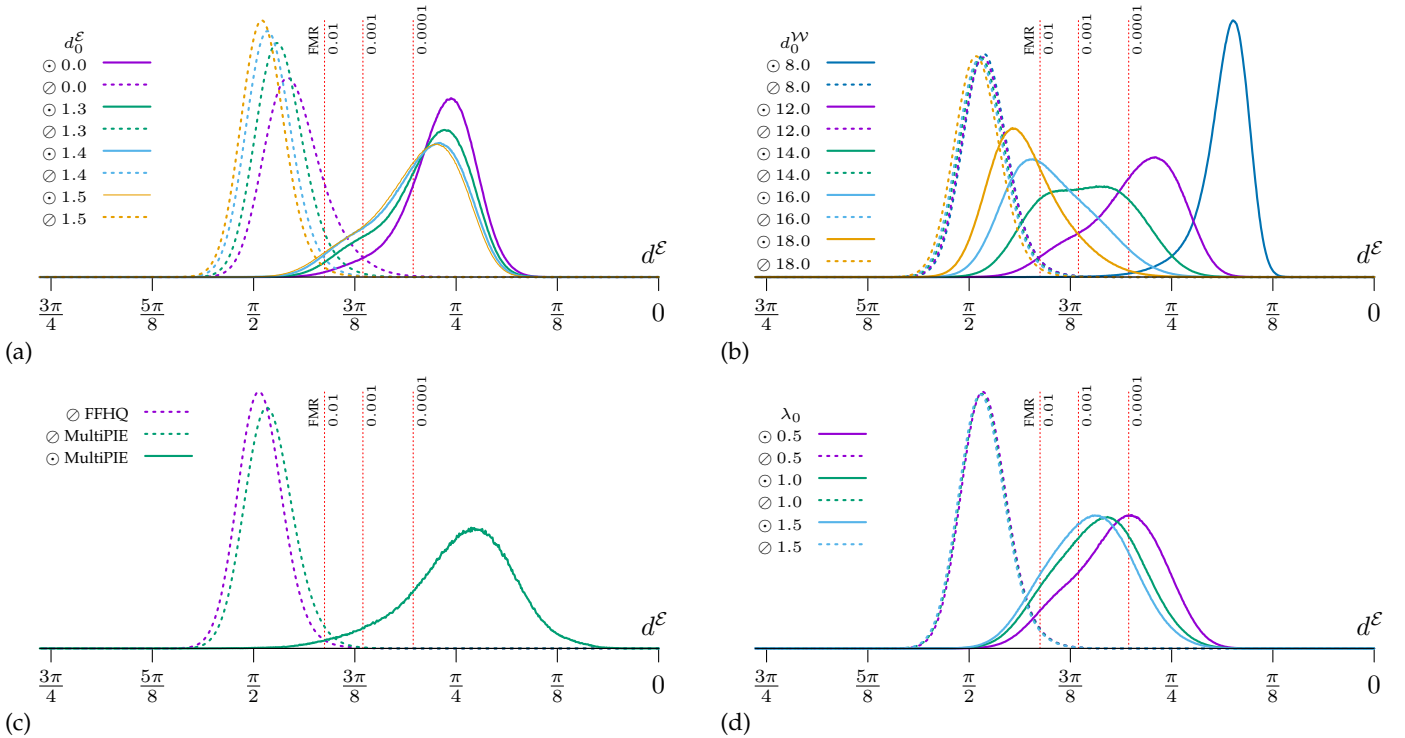


Fig. 6: *intra-class* \odot and *inter-class* \otimes embedding distance histograms of synthetic datasets generated with the *Langevin*, *Dispersion* and *DisCo* algorithms as well as genuine real-world data. In (a), the *Langevin* repulsion distance d_0^E is shown to affect the *inter-class* distance statistics. In (b) and (d), the *Dispersion* repulsion distance d_0^{WV} and *DisCo* scale λ_0 are shown to affect the *intra-class* distance statistics. In (c), genuine datasets histograms are shown for comparison. The vertical dashed lines, denoted “FMR”, show the distances for the reference FR backbone evaluated on IJB-C dataset for three different FMR values.

TABLE 7: Influence of *Dispersion* repulsion distance threshold d_0^{WV} on FR accuracy.

d_0^{WV}	N_{iter}	LFW	CPLFW	CALFW	CFP	AgeDB	Average
8.0	20	84	59.57	70.62	59.99	63.57	67.55
12.0	20	94.43	65.08	85.13	65.6	76.97	77.44
14.0	20	96.48	65.62	89.53	67.9	83.93	80.69
16.0	20	96.15	62.47	88.43	67.54	82.83	79.48
18.0	20	95.25	63.3	87.12	66.41	81.2	78.66
20.0	20	54.33	50.07	49.83	55.04	51.68	52.19

these two parameters. Table (6) and Table (7) show such a survey, for five different values of d_0^E and six different values of d_0^{WV} . As we can see from the first table, the values $d_0^E = 1.4$ and $d_0^E = 1.5$ of the *Langevin* repulsion distance threshold yield the best FR performance, while further increasing this parameter to $d_0^E = 1.6$ degrades the overall performance. As we can see by comparing peaks of pairwise *inter-class* distances histograms of genuine and synthetic data in Fig. (6), these best performing parameters values yield distributions close to genuine data from the *FFHQ* and *MultiPIE* datasets. Keeping the fixed value $d_0^E = 1.4$, we see from the second table that the best performance is achieved with the parameter value $d_0^{WV} = 14.0$. It is interesting to note that the values $d_0^{WV} = 12.0$, $d_0^{WV} = 16.0$ and $d_0^{WV} = 18.0$ yields almost similar performance figures, but with widely different pairwise distances distributions.

In section 3 we introduced a modification of *Dispersion*, the *DisCo* algorithm, that initialize the *intra-class* variations

TABLE 8: Influence of *DisCo* parameter λ_0 on FR accuracy.

d_0^{WV}	λ_0	LFW	CPLFW	CALFW	CFP	AgeDB	Average
12.0	0.0	94.43	65.08	85.13	65.6	76.97	77.44
12.0	0.5	95.65	69.6	87.45	68.54	80.32	80.31
12.0	1.5	96.2	73.25	87.7	73.89	80.73	82.35
12.0	1.0	96.6	74.77	87.77	73.89	80.7	82.75
14.0	1.5	97.22	75.85	89.48	78.76	83.32	84.93
16.0	2.0	94.82	65.18	85.00	72.39	77.27	78.93

with a random linear combination of the *covariates* vectors introduced in [13]. This modification is introduced to further increase the *intra-class* variability of the final datasets and the implementation introduces an additional parameter λ_0 that controls the scale of the random weights $\lambda_{aI}^\alpha \in [-\lambda_0, \lambda_0]$. Table (8) shows the performance of five such ensembles compared to the pure *Dispersion* baseline $\lambda_0 = 0$. The first three datasets use a latent repulsion distance of $d_0^{WV} = 12.0$ while the fourth and last further increase this parameter. As demonstrated by the results in this table, this algorithm yields significant performance improvement compared to the original one using purely random initialization, at least up to a value of $\lambda_0 = 1.5$. This gain is of between two and four percents for the LFW, CALFW and AgeDB benchmarks, which is already quite significant. Where the *DisCo* yields the biggest advantage however is on the CPLFW and CFP benchmarks, where improvements of up to twelve percents are observed. This indicates that the *DisCo* algorithm helps generates more diversity, and that it

TABLE 9: Influence of training set repulsion on FR accuracy.

$d_{tr}^{\mathcal{E}}$	$d_0^{\mathcal{E}}$	LFW	CPLFW	CALFW	CFP	AgeDB	Average
0.0	1.4	94.43	65.08	85.13	65.6	76.97	77.44
0.6	1.4	94.97	65.15	85.62	65.19	78.42	77.87
0.8	1.4	94.95	66.28	86.5	65.24	78.9	78.37
1.0	1.4	94.77	65.23	86.22	66.61	78.33	78.23
1.2	1.4	94.95	65.08	85.97	65.56	79.07	78.13
1.3	1.4	94.58	65.18	86.37	65.91	79.85	78.38
1.4	1.4	94.08	65.62	85.37	66.93	77.12	77.82
1.5	1.4	91.85	64.58	81.58	66.37	71.72	75.22

is helpful in mitigating the relatively poor performances of StyleGAN2 ensembles on pose benchmarks.

4.6 Generator Training Set Leakage and Mitigation

While we have generated a large quantity of synthetic data, it is important to emphasize that both the generator and the reference FR model are trained on genuine data. It is important to verify that the synthetic data generated by our algorithms is sufficiently far away from the original genuine training sets and, if it is not the case, find appropriate mitigation techniques to control potential *training set leakage*. We have observed that, despite the care taken by the authors of the DCFace dataset [8], their method still generate a significant number of samples that are very close, if not indistinguishable, from pictures from the generator training set.

One possible option to mitigate this problem, and protect the privacy of the real-world identities present in the training set, is to repulse the synthetic samples embeddings from the embedding of the training set samples. This is quite easily implemented in *Langevin* by adding a loss function similar to Eq. (10) but with the pairwise distances $d^{\mathcal{E}}(e_a, E_b)$ of the synthetic embeddings e_a to the genuine ones E_b . For this, we introduce a new parameter $d_{tr}^{\mathcal{E}}$ which is similar to the pairwise embedding repulsion distance $d_0^{\mathcal{E}}$ but for granular interactions between synthetic and genuine samples. Table (9), shows the results of this undertaking, for several values of $d_{tr}^{\mathcal{E}}$. We observe that, surprisingly, increasing the value $d_{tr}^{\mathcal{E}}$ slightly increases FR accuracy, and the biggest value considered $d_{tr}^{\mathcal{E}} = 1.3$ performs slightly better than no training set repulsion at all. While we keep a more detailed study of this phenomenon for a subsequent publication, we note that this method seems to be a promising avenue for biometric privacy research, for synthetic data at least.

4.7 Closing the Gap with Real-World Data

Having performed a detailed analysis of the *Langevin*, *Dispersion* and *DisCo* algorithms as well as the influence of their respective parameters, we are now interested to see if we can scale our approach to bigger synthetic datasets. Table (10) shows the result of this survey. In this table, we also show the effect of compounded datasets, datasets that have the same biometric references, created with *Langevin*, but different variations. In particular, several datasets are compounded with their reference *Langevin* ensemble, thus adding one variation per class, denoted by a check-mark in the Ref. column of the table. As we can see, this offers a very limited performance increase but we decide to keep this for bigger datasets as the data has to be computed anyway.

Scaling up to $N_{id} = 30k$ however offers an impressive performance improvement, in particular with *DisCo* variations, with an impressive average score of 88.40, almost reaching the performance of diffusion based methods. For $N_{id} = 30k$ we also study the influence of the number of variations, showing that $N_{var} = 64$ yields the best results. Surprisingly, for $N_{var} = 128$ the performance drops very significantly, by almost twenty points. This might be explained by the lack of *inter-class latent repulsion*, a design choice made for simplicity, as explained previously. To better assess the performance of our best datasets, Fig. (7) shows the Receiver Operating Characteristic (ROC) curves for a number of models trained on synthetic and genuine data. As can be observed in this figure, our method outperforms all GAN-based synthetic datasets in the literature. In addition, our method achieves comparable performance with diffusion-based datasets for high values of FMR; however, for low values of FMR, diffusion-based methods achieve better performance than our method. We should note that, as mentioned in section 2, DCFace is generated with a dual condition model trained on CASIA-WebFace [6] with identity labels, and therefore the generator model leverages⁴ the identity information in the CASIA-WebFace dataset. In contrast, our method is based on a pretrained generative model, which is trained on unlabeled face images from the FFHQ dataset. Compared to FR models trained with real data, the ROC curves show that there is still a gap between training with real and synthetic datasets. Nevertheless, the promising improvement achieved by our method for GAN-based models reveals potential in generative models and training FR with synthetic data, which require further research in the future.

5 CONCLUSIONS

5.1 Conclusions

We have developed new techniques to generate large-scale face images datasets using GANs. These methods involve physics-inspired algorithms to sample synthetic identities in the latent space of a generative network. In particular, we believe that our use of loss functions inspired by granular mechanics is quite novel in this context and open promising avenues, possibly beyond face recognition applications.

This work introduced three complementary algorithms, *Langevin*, *Dispersion* and *DisCo*, aimed at generating large synthetic datasets to replace, at least partially, genuine face datasets captured *in the wild* and to mitigate ethical issues arising from their usage. These algorithms take inspiration from physical processes such as *Brownian motion* and granular media *contact interactions* to generate ensembles of samples in the latent space of generative models. For this work we focussed on GANs, but these methods can be generalized to any model with a latent space of reasonable dimensionality. Importantly, these algorithms introduce a

4. Since DCFace is trained on CASIA-WebFace dataset with identity labels, the recent Synthetic Data for Face Recognition (SDFR) Competition held in conjunction with the 18th IEEE International Conference on Automatic Face and Gesture Recognition (FG 2024) disqualified all submissions based on DCFace [75].

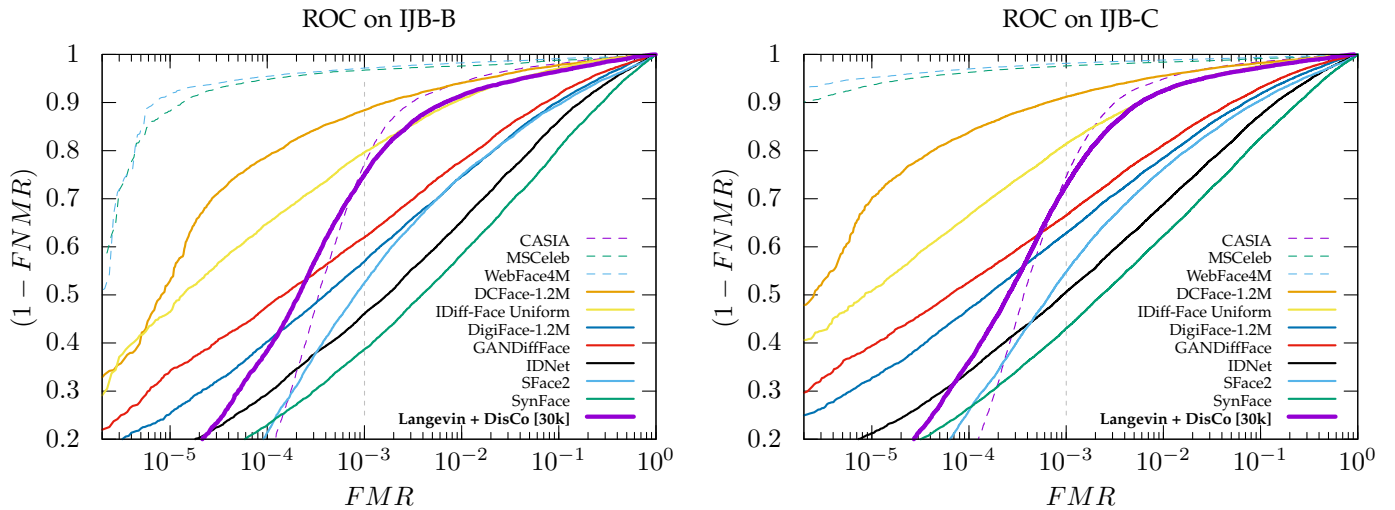


Fig. 7: ROC curves for models trained on synthetic datasets, benchmarked on the IJB-B and IJB-C datasets.

TABLE 10: Influence of the number of identities, number of variations and variation-creation method on FR accuracy.

Method	N_{id}	N_{img}	Ref. [†]	N_{var}	$d_0^{\mathcal{V}}$	λ_0	LFW	CPLFW	CALFW	CFP	AgeDB	Average
<i>Langevin + Dispersion</i>	10'000	640'000	-	64	12.0	-	94.43	65.08	85.13	65.6	76.97	77.44
		650'000	✓	64 + 1	12.0	-	94.38	65.75	86.03	65.51	77.3	77.79
	30'000	480'000	-	16	12.0	-	90.65	64.42	80.12	63.07	70.18	73.69
		960'000	-	32	12.0	-	94.83	66.25	84.3	65.51	76.1	77.40
<i>Langevin + DisCo</i>	10'000	640'000	-	64	12.0	-	96.6	74.77	87.77	73.89	80.7	82.75
		1'300'000	✓	64 + 1	12.0	1.5	98.22	77.57	91.93	78.93	89.95	87.32
	20'000	1'300'000	✓	64 + 1	14.0	1.5	98.53	81.17	92.93	83.56	92.32	89.70
		1'650'000	✓	64 + 1	12.0	1.5	98.37	79.53	92.58	80.71	90.82	88.40
	30'000	3'870'000	✓	128 + 1	12.0	1.5	86.15	61.98	70.35	68.23	59.87	69.32
		1'470'000	✓	48 + 1	14.0	1.5	98.55	81.32	93.33	83.37	92.05	89.72
		1'650'000	✓	64 + 1	14.0	1.5	98.97	81.52	93.95	83.77	93.32	90.31
		40'000	2'600'000	✓	64 + 1	12.0	1.5	98.33	78.25	92.27	79.31	89.43
	50'000	3'250'000	✓	64 + 1	12.0	1.5	98.47	79.88	92.57	79.93	90.33	88.24
	<i>Langevin + Covariates</i>	10'000	180'000	✓	17 + 1	-	-	77.68	59.2	64.07	61.07	52.55

[†] References created with *Langevin* are compounded with the variations for FR model training.

set of free parameters that control the distribution of samples in the latent space and which can be optimized to yield high quality synthetic datasets tailored for specific usages.

To validate the soundness of our approach and evaluate its effectiveness at generating useful synthetic face data, we trained FR models on the synthetic datasets we generated and evaluated the resulting models on seven standard face biometric benchmarks. With these results, we showed that the face datasets we can generate greatly outperform previous GANs generated ones while almost reaching the current *state of the art* performance of synthetic datasets generated with diffusion models. We are confident that the results of this preliminary study can be further improved, possibly quite significantly.

While we showed that our algorithms can yield very good synthetic face datasets, many improvements are still to be made. Most importantly, our method crucially relies on a reference off-the-shelf FR model. In some sense, the datasets generated with our method iteratively *learns*, by stochastic gradient descent, from the reference FR model, and therefore quite certainly learn its biases as well. A possible fix that could mitigate, at least partially, this fundamental issue is to use several reference models in parallel, simply by adding more embedding losses to the algorithms.

Fundamentally, the problem of generating complex synthetic data, that has similar characteristics that some genuine reference, is a *chicken-and-egg* problem. It could be perhaps constructive to reformulate this problem in a way that makes it clear that the synthetic data will always depends to some extent on genuine priors, and rather insist on developing procedures giving guaranties that the original data is at least hard to recover and that the synthetic dataset gives a good enough representation of reality. A few steps in this direction were performed at the end of section 4, possibly also hinting at some interesting research directions toward a much deeper problem: generalization of DL models.

We would like to stress that, while large part of this work was devoted to optimization of these algorithms, they remain quite expensive, computationally speaking. For each sample an image must be generated and its embedding computed, twice per iteration with one backward pass, which is quite expensive as the data goes through an intermediary image space of very high dimensionality. On the other hand the only function we are interested in is an identity aware metric $d_{id}^{\mathcal{V}}$ on the latent space of a given generator. It is certainly possible to learn such a function to a relevant degree of accuracy and to use this instead of the full chain, at least for bootstrapping. Alternatively, while technically

challenging, it is certainly possible to prune connections and weights in the $\mathcal{W} \rightarrow \mathcal{E}$ generator-feature-extractor chain, which would vastly improve efficiency.

5.2 Source Code and Data Availability

To adhere to the strongest standards of reproducible research, the code used for these experiments is made available at the following address under an open-source license. Since generating such datasets is quite computationally expensive, we also provide access to some the synthetic data generated for this work.

[URLs will be added upon acceptance]

REFERENCES

- [1] Y. LeCun, Y. Bengio, and G. Hinton, "Deep learning," *nature*, vol. 521, no. 7553, pp. 436–444, 2015.
- [2] S. Prabhakar, S. Pankanti, and A. K. Jain, "Biometric recognition: Security and privacy concerns," *IEEE security & privacy*, vol. 1, no. 2, pp. 33–42, 2003.
- [3] P. Drozdzowski, C. Rathgeb, A. Dantcheva, N. Damer, and C. Busch, "Demographic bias in biometrics: A survey on an emerging challenge," *IEEE Transactions on Technology and Society*, vol. 1, no. 2, pp. 89–103, 2020.
- [4] Y. Guo, L. Zhang, Y. Hu, X. He, and J. Gao, "Ms-celeb-1m: A dataset and benchmark for large-scale face recognition," in *Computer Vision—ECCV 2016: 14th European Conference, Amsterdam, The Netherlands, October 11–14, 2016, Proceedings, Part III 14*. Springer, 2016, pp. 87–102.
- [5] Z. Zhu, G. Huang, J. Deng, Y. Ye, J. Huang, X. Chen, J. Zhu, T. Yang, J. Lu, D. Du *et al.*, "Webface260m: A benchmark unveiling the power of million-scale deep face recognition," in *Proceedings of the IEEE/CVF Conference on Computer Vision and Pattern Recognition*, 2021, pp. 10 492–10 502.
- [6] D. Yi, Z. Lei, S. Liao, and S. Z. Li, "Learning face representation from scratch," *arXiv preprint arXiv:1411.7923*, 2014.
- [7] G. Bae, M. de La Gorce, T. Baltrušaitis, C. Hewitt, D. Chen, J. Valentin, R. Cipolla, and J. Shen, "Digiface-1m: 1 million digital face images for face recognition," in *Proceedings of the IEEE/CVF Winter Conference on Applications of Computer Vision*, 2023, pp. 3526–3535.
- [8] M. Kim, F. Liu, A. Jain, and X. Liu, "Dcface: Synthetic face generation with dual condition diffusion model," in *Proceedings of the IEEE/CVF Conference on Computer Vision and Pattern Recognition*, 2023, pp. 12 715–12 725.
- [9] F. Boutros, J. H. Grebe, A. Kuijper, and N. Damer, "Idiff-face: Synthetic-based face recognition through fuzzy identity-conditioned diffusion model," in *Proceedings of the IEEE/CVF International Conference on Computer Vision*, 2023, pp. 19 650–19 661.
- [10] H. Qiu, B. Yu, D. Gong, Z. Li, W. Liu, and D. Tao, "Synface: Face recognition with synthetic data," in *Proceedings of the IEEE/CVF International Conference on Computer Vision*, 2021, pp. 10 880–10 890.
- [11] F. Boutros, M. Huber, P. Siebke, T. Rieber, and N. Damer, "Sface: Privacy-friendly and accurate face recognition using synthetic data," in *2022 IEEE International Joint Conference on Biometrics (IJCB)*. IEEE, 2022, pp. 1–11.
- [12] F. Boutros, M. Huber, A. T. Luu, P. Siebke, and N. Damer, "Sface2: Synthetic-based face recognition with w-space identity-driven sampling," *IEEE Transactions on Biometrics, Behavior, and Identity Science*, 2024.
- [13] L. Colbois, T. de Freitas Pereira, and S. Marcel, "On the use of automatically generated synthetic image datasets for benchmarking face recognition," in *2021 IEEE International Joint Conference on Biometrics (IJCB)*. IEEE, 2021, pp. 1–8.
- [14] P. Melzi, C. Rathgeb, R. Tolosana, R. Vera-Rodriguez, D. Lawatsch, F. Domin, and M. Schaubert, "Gandiffface: Controllable generation of synthetic datasets for face recognition with realistic variations," *arXiv preprint arXiv:2305.19962*, 2023.
- [15] J. N. Kolf, T. Rieber, J. Elliesen, F. Boutros, A. Kuijper, and N. Damer, "Identity-driven three-player generative adversarial network for synthetic-based face recognition," in *Proceedings of the IEEE/CVF Conference on Computer Vision and Pattern Recognition*, 2023, pp. 806–816.
- [16] F. Boutros, M. Klemt, M. Fang, A. Kuijper, and N. Damer, "Exface-gan: Exploring identity directions in gan's learned latent space for synthetic identity generation," in *2023 IEEE International Joint Conference on Biometrics (IJCB)*. IEEE, 2023, pp. 1–10.
- [17] Y. Deng, J. Yang, D. Chen, F. Wen, and X. Tong, "Disentangled and controllable face image generation via 3d imitative-contrastive learning," in *Proceedings of the IEEE/CVF conference on computer vision and pattern recognition*, 2020, pp. 5154–5163.
- [18] I. Goodfellow, J. Pouget-Abadie, M. Mirza, B. Xu, D. Warde-Farley, S. Ozair, A. Courville, and Y. Bengio, "Generative adversarial nets," *Advances in neural information processing systems*, vol. 27, 2014.
- [19] A. Creswell, T. White, V. Dumoulin, K. Arulkumaran, B. Sengupta, and A. A. Bharath, "Generative adversarial networks: An overview," *IEEE signal processing magazine*, vol. 35, no. 1, pp. 53–65, 2018.
- [20] T. Karras, S. Laine, and T. Aila, "A style-based generator architecture for generative adversarial networks," in *Proceedings of the IEEE/CVF conference on computer vision and pattern recognition*, 2019, pp. 4401–4410.
- [21] T. Karras, S. Laine, M. Aittala, J. Hellsten, J. Lehtinen, and T. Aila, "Analyzing and improving the image quality of StyleGAN," in *Proc. CVPR*, 2020.
- [22] T. Karras, M. Aittala, S. Laine, E. Härkönen, J. Hellsten, J. Lehtinen, and T. Aila, "Alias-free generative adversarial networks," *Advances in Neural Information Processing Systems*, vol. 34, pp. 852–863, 2021.
- [23] E. R. Chan, C. Z. Lin, M. A. Chan, K. Nagano, B. Pan, S. De Mello, O. Gallo, L. J. Guibas, J. Tremblay, S. Khamis *et al.*, "Efficient geometry-aware 3d generative adversarial networks," in *Proceedings of the IEEE/CVF Conference on Computer Vision and Pattern Recognition*, 2022, pp. 16 123–16 133.
- [24] H. Bai, D. Kang, H. Zhang, J. Pan, and L. Bao, "Ffhq-uv: Normalized facial uv-texture dataset for 3d face reconstruction," in *Proceedings of the IEEE/CVF Conference on Computer Vision and Pattern Recognition*, 2023, pp. 362–371.
- [25] R. Abdal, Y. Qin, and P. Wonka, "Image2stylegan: How to embed images into the stylegan latent space?" in *Proceedings of the IEEE/CVF international conference on computer vision*, 2019, pp. 4432–4441.
- [26] J. Zhu, Y. Shen, D. Zhao, and B. Zhou, "In-domain gan inversion for real image editing," in *European conference on computer vision*. Springer, 2020, pp. 592–608.
- [27] Q. Feng, V. Shah, R. Gadde, P. Perona, and A. Martinez, "Near perfect gan inversion," *arXiv preprint arXiv:2202.11833*, 2022.
- [28] D. Roich, R. Mokady, A. H. Bermano, and D. Cohen-Or, "Pivotal tuning for latent-based editing of real images," *ACM Transactions on graphics (TOG)*, vol. 42, no. 1, pp. 1–13, 2022.
- [29] S. Khodadadeh, S. Ghadar, S. Motiian, W.-A. Lin, L. Bölöni, and R. Kalarot, "Latent to latent: A learned mapper for identity preserving editing of multiple face attributes in stylegan-generated images," in *Proceedings of the IEEE/CVF Winter Conference on Applications of Computer Vision*, 2022, pp. 3184–3192.
- [30] R. Haas, S. Grafshof, and S. S. Brandt, "Tensor-based emotion editing in the stylegan latent space," *arXiv preprint arXiv:2205.06102*, 2022.
- [31] X. Pan, A. Tewari, T. Leimkühler, L. Liu, A. Meka, and C. Theobalt, "Drag your gan: Interactive point-based manipulation on the generative image manifold," *arXiv preprint arXiv:2305.10973*, 2023.
- [32] W. Li, L. Zhang, D. Wang, B. Zhao, Z. Wang, M. Chen, B. Zhang, Z. Wang, L. Bo, and X. Li, "One-shot high-fidelity talking-head synthesis with deformable neural radiance field," in *Proceedings of the IEEE/CVF Conference on Computer Vision and Pattern Recognition*, 2023, pp. 17 969–17 978.
- [33] K. Deng, G. Yang, D. Ramanan, and J.-Y. Zhu, "3d-aware conditional image synthesis," in *Proceedings of the IEEE/CVF Conference on Computer Vision and Pattern Recognition*, 2023, pp. 4434–4445.
- [34] J. Ho, A. Jain, and P. Abbeel, "Denoising diffusion probabilistic models," *Advances in neural information processing systems*, vol. 33, pp. 6840–6851, 2020.
- [35] A. Q. Nichol and P. Dhariwal, "Improved denoising diffusion probabilistic models," in *International Conference on Machine Learning*. PMLR, 2021, pp. 8162–8171.
- [36] C. Saharia, W. Chan, S. Saxena, L. Li, J. Whang, E. L. Denton, K. Ghasemipour, R. Gontijo Lopes, B. Karagol Ayan, T. Salimans *et al.*, "Photorealistic text-to-image diffusion models with deep lan-

- guage understanding," *Advances in Neural Information Processing Systems*, vol. 35, pp. 36 479–36 494, 2022.
- [37] R. Rombach, A. Blattmann, D. Lorenz, P. Esser, and B. Ommer, "High-resolution image synthesis with latent diffusion models," in *Proceedings of the IEEE/CVF conference on computer vision and pattern recognition*, 2022, pp. 10 684–10 695.
- [38] K. Preechakul, N. Chatthee, S. Widadwongsa, and S. Suwanajakorn, "Diffusion autoencoders: Toward a meaningful and decodable representation," in *Proceedings of the IEEE/CVF Conference on Computer Vision and Pattern Recognition*, 2022, pp. 10 619–10 629.
- [39] N. Carlini, J. Hayes, M. Nasr, M. Jagielski, V. Schwag, F. Tramèr, B. Balle, D. Ippolito, and E. Wallace, "Extracting training data from diffusion models," in *32nd USENIX Security Symposium (USENIX Security 23)*, 2023, pp. 5253–5270.
- [40] N. Vyas, S. M. Kakade, and B. Barak, "On provable copyright protection for generative models," in *International Conference on Machine Learning*. PMLR, 2023, pp. 35 277–35 299.
- [41] G. Somepalli, V. Singla, M. Goldblum, J. Geiping, and T. Goldstein, "Diffusion art or digital forgery? investigating data replication in diffusion models," in *Proceedings of the IEEE/CVF Conference on Computer Vision and Pattern Recognition*, 2023, pp. 6048–6058.
- [42] —, "Understanding and mitigating copying in diffusion models," *Advances in Neural Information Processing Systems*, vol. 36, pp. 47 783–47 803, 2023.
- [43] Z. Li, J. Hong, B. Li, and Z. Wang, "Shake to leak: Fine-tuning diffusion models can amplify the generative privacy risk," *arXiv preprint arXiv:2403.09450*, 2024.
- [44] V. Blanz and T. Vetter, "A morphable model for the synthesis of 3d faces," in *Proceedings of the 26th annual conference on Computer graphics and interactive techniques*, 1999, pp. 187–194.
- [45] P. Paysan, R. Knothe, B. Amberg, S. Romdhani, and T. Vetter, "A 3d face model for pose and illumination invariant face recognition," in *2009 sixth IEEE international conference on advanced video and signal based surveillance*. Ieee, 2009, pp. 296–301.
- [46] T. Gerig, A. Morel-Forster, C. Blumer, B. Egger, M. Luthi, S. Schönborn, and T. Vetter, "Morphable face models—an open framework," in *2018 13th IEEE International Conference on Automatic Face & Gesture Recognition (FG 2018)*. IEEE, 2018, pp. 75–82.
- [47] T. Li, T. Bolkart, M. J. Black, H. Li, and J. Romero, "Learning a model of facial shape and expression from 4d scans." *ACM Trans. Graph.*, vol. 36, no. 6, pp. 194–1, 2017.
- [48] R. Li, K. Bladin, Y. Zhao, C. Chinara, O. Ingraham, P. Xiang, X. Ren, P. Prasad, B. Kishore, J. Xing *et al.*, "Learning formation of physically-based face attributes," in *Proceedings of the IEEE/CVF conference on computer vision and pattern recognition*, 2020, pp. 3410–3419.
- [49] T. Khakhulin, V. Sklyarova, V. Lempitsky, and E. Zakharov, "Realistic one-shot mesh-based head avatars," in *European Conference on Computer Vision*. Springer, 2022, pp. 345–362.
- [50] A. Lattas, S. Moschoglou, S. Ploumpis, B. Gecer, J. Deng, and S. Zafeiriou, "Fitme: Deep photorealistic 3d morphable model avatars," in *Proceedings of the IEEE/CVF Conference on Computer Vision and Pattern Recognition*, 2023, pp. 8629–8640.
- [51] E. Wood, T. Baltrušaitis, C. Hewitt, S. Dziadzio, T. J. Cashman, and J. Shotton, "Fake it till you make it: face analysis in the wild using synthetic data alone," in *Proceedings of the IEEE/CVF international conference on computer vision*, 2021, pp. 3681–3691.
- [52] Y. Deng, J. Yang, S. Xu, D. Chen, Y. Jia, and X. Tong, "Accurate 3d face reconstruction with weakly-supervised learning: From single image to image set," in *Proceedings of the IEEE/CVF conference on computer vision and pattern recognition workshops*, 2019, pp. 0–0.
- [53] B. Mildenhall, P. P. Srinivasan, M. Tancik, J. T. Barron, R. Ramamoorthi, and R. Ng, "Nerf: Representing scenes as neural radiance fields for view synthesis," *Communications of the ACM*, vol. 65, no. 1, pp. 99–106, 2021.
- [54] N. Ruiz, Y. Li, V. Jampani, Y. Pritch, M. Rubinstein, and K. Aberman, "Dreambooth: Fine tuning text-to-image diffusion models for subject-driven generation," in *Proceedings of the IEEE/CVF Conference on Computer Vision and Pattern Recognition*, 2023, pp. 22 500–22 510.
- [55] A. Shoshan, N. Bhonker, I. Kviatkovsky, and G. Medioni, "Gan-control: Explicitly controllable gans," in *Proceedings of the IEEE/CVF international conference on computer vision*, 2021, pp. 14 083–14 093.
- [56] G. Biroli, "A new kind of phase transition?" *Nature Physics*, vol. 3, no. 4, pp. 222–223, 2007.
- [57] N. Brilliantov, C. Saluena, T. Schwager, and T. Pöschel, "Transient structures in a granular gas," *Physical review letters*, vol. 93, no. 13, p. 134301, 2004.
- [58] P. A. Cundall and O. D. Strack, "A discrete numerical model for granular assemblies," *geotechnique*, vol. 29, no. 1, pp. 47–65, 1979.
- [59] J. Luo, H. Qiao, and B. Zhang, "Learning with smooth hinge losses," *Neurocomputing*, vol. 463, pp. 379–387, 2021.
- [60] A. Einstein, "Über die von der molekularkinetischen theorie der wärme geforderte bewegung von in ruhenden flüssigkeiten suspendierten teilchen," *Annalen der physik*, vol. 4, 1905.
- [61] R. Carmona, H. Kesten, J. B. Walsh, and J. B. Walsh, *An introduction to stochastic partial differential equations*. Springer, 1986.
- [62] R. C. Dalang and M. Sanz-Solé, "An introduction to stochastic partial differential equations: Part i," *arXiv preprint arXiv:2402.02119*, 2024.
- [63] J. Deng, J. Guo, N. Xue, and S. Zafeiriou, "Arcface: Additive angular margin loss for deep face recognition," in *Proceedings of the IEEE/CVF conference on computer vision and pattern recognition*, 2019, pp. 4690–4699.
- [64] H. Cohn, A. Kumar, S. Miller, D. Radchenko, and M. Viazovska, "The sphere packing problem in dimension 24," *Annals of Mathematics*, vol. 185, no. 3, pp. 1017–1033, 2017.
- [65] M. Geiger, S. Spigler, S. d'Ascoli, L. Sagun, M. Baity-Jesi, G. Biroli, and M. Wyart, "Jamming transition as a paradigm to understand the loss landscape of deep neural networks," *Physical Review E*, vol. 100, no. 1, p. 012115, 2019.
- [66] M. Kim, A. K. Jain, and X. Liu, "Adaface: Quality adaptive margin for face recognition," in *Proceedings of the IEEE/CVF conference on computer vision and pattern recognition*, 2022, pp. 18 750–18 759.
- [67] G. B. Huang, M. Mattar, T. Berg, and E. Learned-Miller, "Labeled faces in the wild: A database forstudying face recognition in unconstrained environments," in *Workshop on faces in' Real-Life' Images: detection, alignment, and recognition*, 2008.
- [68] T. Zheng, W. Deng, and J. Hu, "Cross-age lfw: A database for studying cross-age face recognition in unconstrained environments," *arXiv preprint arXiv:1708.08197*, 2017.
- [69] T. Zheng and W. Deng, "Cross-pose lfw: A database for studying cross-pose face recognition in unconstrained environments," *Beijing University of Posts and Telecommunications, Tech. Rep*, vol. 5, no. 7, 2018.
- [70] S. Sengupta, J.-C. Chen, C. Castillo, V. M. Patel, R. Chellappa, and D. W. Jacobs, "Frontal to profile face verification in the wild," in *2016 IEEE winter conference on applications of computer vision (WACV)*. IEEE, 2016, pp. 1–9.
- [71] S. Moschoglou, A. Papaioannou, C. Sagonas, J. Deng, I. Kotsia, and S. Zafeiriou, "Agedb: the first manually collected, in-the-wild age database," in *proceedings of the IEEE conference on computer vision and pattern recognition workshops*, 2017, pp. 51–59.
- [72] C. Whitelam, E. Taborisky, A. Blanton, B. Maze, J. Adams, T. Miller, N. Kalka, A. K. Jain, J. A. Duncan, K. Allen *et al.*, "Iarpa janus benchmark-b face dataset," in *proceedings of the IEEE conference on computer vision and pattern recognition workshops*, 2017, pp. 90–98.
- [73] B. Maze, J. Adams, J. A. Duncan, N. Kalka, T. Miller, C. Otto, A. K. Jain, W. T. Niggel, J. Anderson, J. Cheney *et al.*, "Iarpa janus benchmark-c: Face dataset and protocol," in *2018 international conference on biometrics (ICB)*. IEEE, 2018, pp. 158–165.
- [74] A. Anjos, M. Günther, T. de Freitas Pereira, P. Korshunov, A. Mohammadi, and S. Marcel, "Continuously reproducing toolchains in pattern recognition and machine learning experiments," 2017.
- [75] H. O. Shahreza *et al.*, "Sdfr: Synthetic data for face recognition competition," *arXiv preprint arXiv:2404.04580*, 2024.